arXiv:0908.2922v1 [cond-mat.stat-mech] 20 Aug 2009

1

Non-equilibrium dynamics of quantum systems: order parameter evolution, defect generation, and qubit transfer

Shreyoshi Mondal[(1)], Diptiman Sen[(2)] and K. Sengupta[(1,3)]

[(1)] Theoretical Physics Department, Indian Association for the Cultivation of Sciences, Jadavpur, Kolkata 700 032, India
[(2)] Center for High Energy Physics, Indian Institute of Science, Bangalore 560 012, India
[(3)] Theoretical Condensed Matter Physics Division, Saha Institute of Nuclear Physics, 1/AF Bidhannagar, Kolkata 700 064, India

1.1 Introduction

The properties of systems near quantum critical points (QCPs) have been studied extensively in recent years [1, 2]. A QCP is a point across which the symmetry of the ground state of a quantum system changes in a fundamental way; such a point can be accessed by changing some parameter, say λ, in the Hamiltonian governing the system. The change in the ground state across a QCP is mediated by quantum fluctuations. Unlike conventional thermal critical points, thermal fluctuations do not play a crucial role in such transitions. Similar to its thermal counterparts, the low energy physics near a QCP is associated with a number of critical exponents which characterize the universality class of such a transition. Amongst these exponents, the dynamical critical exponent z provides the signature of the relative scaling of space and time at the transition and has no counterpart in thermal phase transitions. The other exponent which is going to be important for the purpose of this review is the well-known correlation length exponent ν. These exponents are formally defined as follows. As we approach the critical point at $\lambda = \lambda_c$, the correlation length diverges as $\xi \sim |\lambda - \lambda_c|^{-\nu}$, while the gap between the ground state and first excited state vanishes as $\Delta E \sim \xi^{-z} \sim |\lambda - \lambda_c|^{z\nu}$. Exactly at the critical point $\lambda = \lambda_c$, the energy of the low-lying excitations vanishes at some wave number $\mathbf{k}_0$ as $\omega \sim |\mathbf{k} - \mathbf{k}_0|^z$. The critical exponents are independent of the details of the microscopic Hamiltonian; they depend only on a few parameters such as the dimensionality of the system and the symmetry of the order parameter. These features render the low energy equilibrium physics of a quantum system near a QCP truly universal.

In contrast to this well-understood universality of the equilibrium properties of a system near a QCP, relatively few universal features are known in the non-equilibrium behavior of a quantum system. Initial studies in this field aimed at understanding the near-equilibrium finite temperature dynamics near a quantum critical

point using the Boltzman equation approach [3]. Such a dynamics is useful in making contact with experiments which are always carried out at finite temperature. Moreover, the excitations near a quantum critical critical point with a non-zero value of η do not have a simple pole structure like that of the conventional quasiparticle excitations of condensed matter systems; this property makes such a dynamics interesting in its own right.

More recently, significant theoretical [4, 5, 6, 7, 8] and experimental [9] endeavors have focussed on out-of-equilibrium dynamics of closed quantum critical systems. On the experimental front, it has been possible, in ultracold atom systems, to gain unprecedented control over the measurement of out-of-equilibrium properties of quantum systems [9]. On the theoretical front, such studies can be broadly classified into two distinct categories. The first type involves a study of the time evolution of a quantum system after a rapid quench through a quantum critical point. Such a study yields information about the order parameter dynamics across a quantum critical point. It turns out that such a dynamics exhibits a universal signature of the quantum critical point crossed during the quench. The second type involves a study of defect production during slow non-adiabatic dynamics through a quantum critical point. Such a defect production mechanism was first pointed out for dynamics through thermal critical points in Refs. [10, 11]. For a slow enough quenches through quantum critical points, the density of defects produced are known to depend on z and ν which characterize the critical point [12, 13, 14].

Quantum communication in spin systems has also been a subject of intense study recently. Following the seminal work in Ref. [15], a tremendous amount of theoretical effort has been put in to understand the nature of qubit transfer through one- or multi-dimensional spin systems [16]. One of the major goals of such studies is to characterize the fidelity of the transfer of a qubit across such a spin system. The maximization of both the fidelity and the speed of transfer, in moving a qubit through a spin chain, is an issue of great interest in such studies.

In this article, we will review some studies of sudden and slow zero temperature non-equilibrium dynamics of closed quantum systems across critical points. In Sect. 1.2, we consider a sudden quench across a quantum critical point. We study the order parameter dynamics of one-dimensional ultracold atoms in an optical lattice in Sect. 1.2.1 and of the infinite range ferromagnetic Ising model in Sect. 1.2.2. We demonstrate that the dynamics shows universal signatures of the QCP across which the system is quenched. In Sect. 1.3, we discuss defect production for slow non-adiabatic dynamics; typically, we find that the density of defects scales as an inverse power of the quench time τ, where the power depends on the dimensionality d of the system, and the exponents z and ν. In Sect. 1.3.1, we discuss the time evolution of the system across a quantum critical surface; we find that the defect scaling exponent in this case depends on the dimensionality of the critical surface. This is confirmed by a study of defect production in the Kitaev model, which is an exactly solvable model of spin-1/2's on a honeycomb lattice. In Sect. 1.3.2, we study the effect of quenching across a QCP in a non-linear way; we find that the defect scaling exponent also depends on the degree of non-linearity. We illustrate these ideas by studying two exactly solvable spin-1/2 models in one dimension. In Sect. 1.3.3, we discuss

a number of experimental systems where our results on defect scaling can possibly be checked. Finally, in Sect. 1.4, we show that non-equilibrium dynamics, in one- and two-dimensional Heisenberg spin models, can be engineered to maximize the fidelity and speed of the transfer of qubits.

1.2 Quench dynamics

1.2.1 Ultracold atoms in an optical lattice

In this section, we shall study a system of ultracold spinless bosons in a one-dimensional (1D) optical lattice in the presence of a harmonic trap potential [17]. We will restrict ourselves to the Mott phase of the bosons and will study their response to a shift in the position of the trap potential. Such a shift acts as an effective "electric field" for the bosons whose Hamiltonian is given by [17]

$$\mathscr{H} \;=\; -t\,\sum_{ij}\left(b_i^\dagger b_j + b_j^\dagger b_i\right) \;+\; \frac{U}{2}\,\sum_i n_i(n_i-1) \;-\; E\,\sum_i \mathbf{e}\cdot\mathbf{r}_i n_i, \tag{1.1}$$

where ij represents pairs of nearest neighbor sites of the optical lattice, $n_i = b_i^\dagger b_i$ is the number operator for the bosons, $\mathbf{r}_i$ are the dimensionless spatial coordinates of the lattice sites (the lattice spacing is unity), $\mathbf{e}$ is a unit vector in the direction of the applied electric field, and the effective electric field E (in units of energy) can be deduced from the shift a of the center of the trap as $E = -a\partial V_{trap}(x)/\partial x$. In what follows, we will restrict ourselves to $|U-E|, t \ll E, U$. We note that such a regime has been achieved in experiments [9].

In the presence of such an electric field, our classical intuition suggests that all the bosons would gather in the last site of the 1D chain thereby minimizing their energy. However, this does not happen for two reasons. First, the bosons are interacting and a state where all the bosons are in a single site leads to a huge interaction energy cost. But more importantly, even non-interacting bosons (or in the parameter regime $E \gg Un_0$ for interacting bosons) do not exhibit this behavior. To understand this, we note that when $U = 0$, $\mathscr{H}$ is simply the Wannier-Stark Hamiltonian whose wave functions, in the limit of strong electric fields ($t \ll E$), are well localized Bessel functions. Thus for $E \gg t$, the bosons remain localized in their respective lattices. It turns out that for realistic optical lattices where interband energy spacings are large compared to both U and E, the Zener tunneling time, i.e., the time taken by the bosons to reach the final ground from this metastable Mott state, is of the order of milliseconds and is larger than the system lifetime [9]. Our strategy will therefore be to start from the parent Mott state of these localized bosons, identify the complete set of states resonantly coupled to this parent state, obtain the effective Hamiltonian within the subspace of these states, and determine its spectrum and correlations. This effective Hamiltonian is expected to describe the low energy behavior of the system.

The parent Mott state and its resonant dipole excitations are shown in Figs. 1.1 and 1.2 [17]. A dipole here consists of a bound pair of hole at site i and an additional

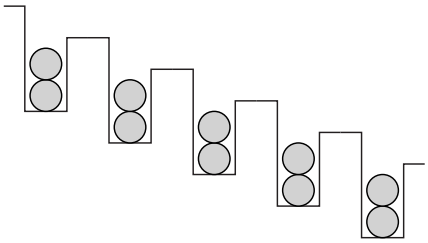

Fig. 1.1. Schematic representation of the parent Mott insulating state with $n_0 = 2$. Each well represents a local minimum of the optical lattice potential — we number these as 1-5 from the left. The potential gradient leads to a uniform decrease in the on-site energy of an atom as we move to the right. The grey circles are the d_i bosons of Eq. (1.2). The vertical direction represents increasing energy: the repulsive interaction energy between the atoms is realized by placing atoms vertically within each well, so that each atom displaces the remaining atoms upwards along the energy axis. We have chosen the diameter of the atoms to equal the potential energy drop between neighboring wells — this corresponds to the condition $U = E$. Consequently, *a resonant transition is one in which the top atom in a well moves horizontally to the top of a nearest neighbor well*; motions either upwards or downwards are non-resonant.

particle at its neighboring $i+1$ site. We note that the dipole excitations cost an energy $U-E$ and hence become energetically favorable when the electric field exceeds the interaction energy. However, once a dipole forms between two adjacent sites, these sites cannot participate in the formation of another dipole since the resultant state lies out of the resonant subspace [17]. This leads to a constraint on the dipole number on any given link ℓ connecting two sites, namely, $n^d_\ell \leq 1$. Similar reasoning, elaborated in Ref. [17], shows that there can be at most one dipole on two adjacent links: $n^d_\ell n^d_{\ell+1} = 0$. The effective Hamiltonian of these dipoles can be written in terms of the dipole annihilation and creation operators d_ℓ and $d^\dagger_\ell$ as

$$\mathscr{H}_d \;=\; -t\sqrt{n_0(n_0+1)}\,\sum_\ell \left(d_\ell + d^\dagger_\ell\right) \;+\; (U-E)\,\sum_\ell d^\dagger_\ell d_\ell. \tag{1.2}$$

Note that the presence of boson hopping leads to non-conservation of the dipole number since such a hopping can spontaneously create or destroy dipoles on a given link. Also, $\mathscr{H}_d$ needs to be supplemented by the constraint conditions $n^d_\ell \leq 1$ and $n^d_\ell n^d_{\ell+1} = 0$.

The phase diagram of the dipolar system can be easily found by inspecting $\mathscr{H}_d$. For $(U-E)/t = \lambda \to \infty$, the ground state of the system represents a vacuum of dipoles. In contrast, for $\lambda \to -\infty$, the ground state is doubly degenerate because there are two distinct states with maximal dipole number: $(\cdots d^\dagger_1 d^\dagger_3 d^\dagger_5 \cdots)|0\rangle$ and $(\cdots d^\dagger_2 d^\dagger_4 d^\dagger_6 \cdots)|0\rangle$. This immediately suggests the existence of an Ising QCP at some intermediate value of λ, associated with an order parameter $\Delta = \sum_\ell (-1)^\ell d^\dagger_\ell d_\ell$ which is a density wave of dipoles with a period of 2 lattice spacings. Further analytic evidence for an Ising QCP can be obtained by examining the excitation spectra for the limiting λ regimes, and noting their similarity to those on either side of the critical point in the quantum Ising chain [1].

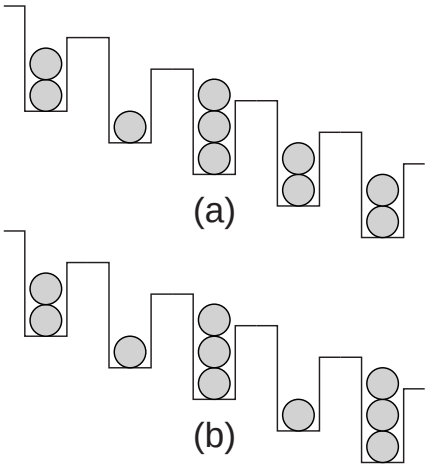

Fig. 1.2. Notation as in Fig. 1.1. (*a*) A dipole on sites 2 and 3; this state is resonantly coupled by an infinitesimal t to the Mott insulator in (*a*) when $E = U$. (*b*) Two dipoles between sites 2 and 3 and between 4 and 5; this state is connected via multiple resonant transitions to the Mott insulator for $E = U$.

For $\lambda \to \infty$, the lowest excited states are single dipoles: $|\ell\rangle = d_\ell^\dagger|0\rangle$. There are N such states (where N is the number of sites), and, at $\lambda = \infty$, they are all degenerate with energy $U - E$. The degeneracy is lifted at second order in a perturbation theory in $1/\lambda$. By a standard approach using canonical transformations, these corrections can be described by an effective Hamiltonian, $\mathscr{H}_{d,\mathrm{eff}}$, which acts entirely within the subspace of single dipole states. We find that

$$\mathscr{H}_{d,\mathrm{eff}} = (U-E)\sum_\ell \Big[|\ell\rangle\langle\ell| + \frac{n_0(n_0+1)}{\lambda^2}\left(|\ell\rangle\langle\ell| + |\ell\rangle\langle\ell+1| + |\ell+1\rangle\langle\ell|\right)\Big]. \quad (1.3)$$

Notice that, quite remarkably, a local dipole hopping term has appeared in the effective Hamiltonian. The constraints ($n_\ell^d \le 1$ and $n_\ell^d n_{\ell+1}^d = 0$) played a crucial role in the derivation of (1.3). Upon considering perturbations to $|\ell\rangle$ from the first term in (1.2), it initially seems possible to obtain an effective matrix element between any two states $|\ell\rangle$ and $|\ell'\rangle$. However this connection can generally happen via two possible intermediate states, $|\ell\rangle \to d_\ell^\dagger d_{\ell'}^\dagger|0\rangle \to |\ell'\rangle$ and $|\ell\rangle \to |0\rangle \to |\ell'\rangle$, and the contributions of the two processes exactly cancel each other for most ℓ, ℓ'. Only when the constraints block the first of these processes is a residual matrix element possible. It is a simple matter to diagonalize $\mathscr{H}_{d,\mathrm{eff}}$ by going to momentum space; we then find a single band of dipole states. The lowest energy dipole state has momentum π: the softening of this state upon reducing λ is then consistent with the appearance of a density wave order with period 2. The higher excited states at large λ consist of multiparticle continua of this band of dipole states, just as in the Ising chain [1]. A related analysis can be carried out for $\lambda \to -\infty$, and the results are similar to those for the ordered state in the quantum Ising chain [1]. The lowest excited states form

a single band of domain walls between the two filled dipole states, and above them are the corresponding multiparticle continua. At an intermediate critical electric field $E_c = U + 1.310t\sqrt{n_0(n_0+1)}$, the system undergoes a quantum phase transition lying in the Ising universality class [17].

Having obtained the equilibrium phase diagram for the model, we now consider the quench dynamics of the dipoles when the value of the electric field is suddenly quenched [4]. We assume that the atoms in the 1D lattice are initially in the ground state $|\Psi_G\rangle$ of the dipole Hamiltonian (1.1) with $E = E_i \ll E_c$. This ground state corresponds to a dipole vacuum. Consider shifting the center of the magnetic trap so that the new potential gradient is E_f. If this change is done suddenly, the system initially remains in the old ground state. The state of the system at time t is therefore given by

$$|\Psi(t)\rangle = \sum_n c_n \exp(-i\varepsilon_n t)|n\rangle, \tag{1.4}$$

where $|n\rangle$ denotes the complete set of energy eigenstates of the Hamiltonian $\mathscr{H}_d$ with $E = E_f$, $\varepsilon_n = \langle n|\mathscr{H}_d[E_f]|n\rangle$ is the energy eigenvalue corresponding to state $|n\rangle$, and $c_n = \langle n|\Psi(t=0)\rangle = \langle n|\Psi_G\rangle$ denotes the overlap of the old ground state with the state $|n\rangle$. (We have set $\hbar = 1$). Notice that the state $|\Psi(t)\rangle$ is no longer the ground state of the new Hamiltonian. Furthermore, in the absence of any dissipative mechanism, which is the case for ultracold atoms in optical lattices, $|\Psi(t)\rangle$ will never reach the ground state of the new Hamiltonian. Rather, in general, we expect the system to thermalize at long enough times, so that the correlations are similar to those of $H_{1D}[E_f]$ at some finite temperature.

We are now in a position to study the dynamics of the Ising density wave order parameter

$$O = \frac{1}{N}\langle\Psi|\Delta|\Psi\rangle, \tag{1.5}$$

where N is the number of sites. The time evolution of O is given by

$$O(t) \;=\; \frac{1}{N}\sum_{m,n} c_m c_n \;\cos\left[(E_m - E_n)t\right]\; \langle m|\sum_\ell (-1)^\ell d_\ell^\dagger d_\ell|n\rangle. \tag{1.6}$$

Eq. (1.6) is solved numerically using exact diagonalization to obtain the eigenstates and eigenvalues of the Hamiltonian $H_{1\mathrm{D}}[E_f]$. Before resorting to numerics, it is useful to discuss the behavior of $O(t)$ qualitatively. We note that if E_f is close to E_i, the old ground state will have a large overlap with the new one, i.e., $c_m \sim \delta_{m1}$. Hence in this case we expect $O(t)$ to have small oscillations about $O(t=0)$. On the other hand, if $E_f \gg E_c$, the two ground states will have very little overlap, and we again expect $O(t)$ to have a small oscillation amplitude. This situation is in stark contrast with the adiabatic turning on of the potential gradient, where the systems always remain in the ground state of the new Hamiltonian $H_{1\mathrm{D}}[E_f]$, and therefore has a maximal value of $\langle O\rangle$ for $E_f \gg E_c$. In between, for $E_f \sim E_c$, the ground state $|\Psi\rangle$ has a finite overlap with many states $|m\rangle$, and hence we expect $O(t)$ to display significant oscillations. Furthermore, if the symmetry between the two Ising ordered states is broken slightly (as is the case in our studies below), the time averaged value of $O(t)$ will be non-zero.

This qualitative discussion is supported by numerical calculations for finite size systems with size $N = 9, 11, 13$. For numerical computations with finite systems, we choose systems with an odd number of sites and open boundary conditions, so that dipole formation on odd sites is favored, thus breaking the Z_2 symmetry. The results are shown in Figs. 1.3 - 1.6.

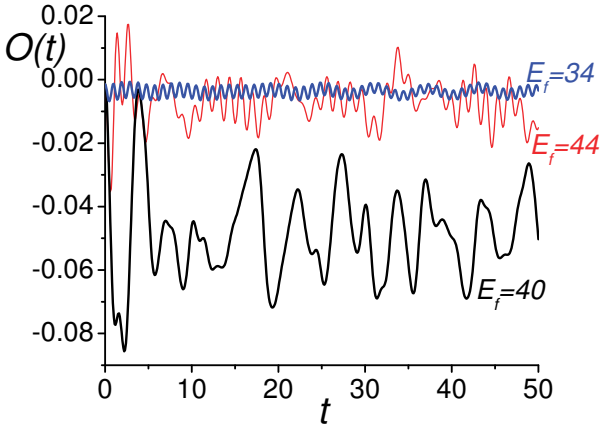

Fig. 1.3. Evolution of the Ising order parameter in (1.5) under the Hamiltonian $H_{1D}[E_f]$ for $n_0 = 1$. The initial state is the ground state of $H_{1D}[E_i]$. All the plots in this section have $U = 40$, $t = 1$, and $E_i = 32$, and consequently the equilibrium QCP is at $E_c = 41.85$.

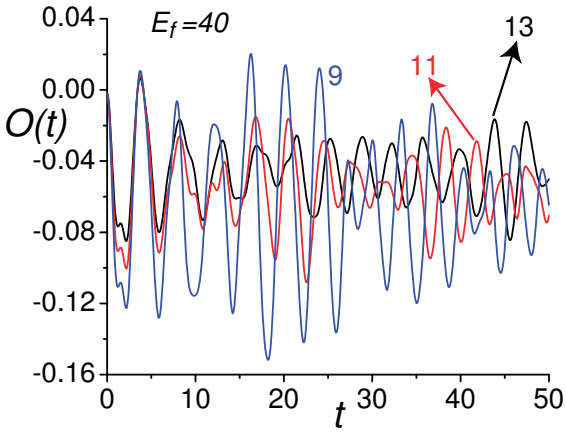

Fig. 1.4. System size (N) dependence of the results of Fig. 1.3 for $E_f = 40$. The curves are labeled by the value of N.

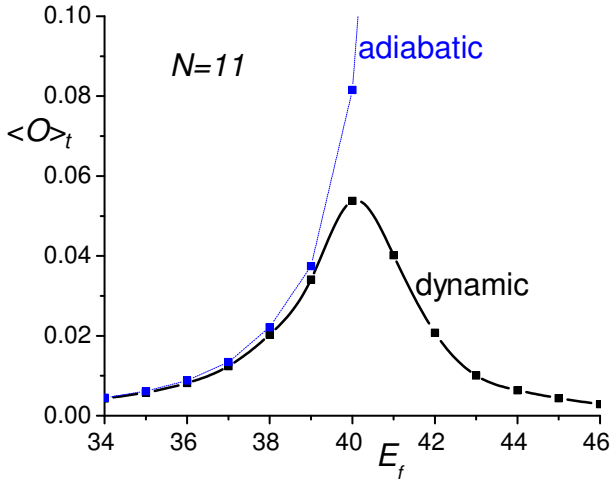

Fig. 1.5. The curve labeled 'dynamic' is the long-time limit $\langle O\rangle_t$ of the Ising order parameter in (1.6) as a function of E_f (for $N = 11$), with other parameters as in Fig. 1.1. This long-time limit can be obtained simply by setting $m = n$ in (1.6). For comparison, in the curve labeled 'adiabatic', we show the expectation value of the Ising order O in the ground state of $H_{1D}[E_f]$; such an order would be observed if the value of E was changed adiabatically. Note that the dynamic curve has its maximal value near (but not exactly at) the equilibrium QCP $E_c = 41.85$, where the system is able to respond most easily to the change in the value of E; this dynamic curve is our theory of the 'resonant' response in the experiments of Ref. [9] discussed in Sect. 1.1. In contrast, the adiabatic result *increases monotonically* with E_f into the $E > E_c$ phase where the Ising symmetry is spontaneously broken.

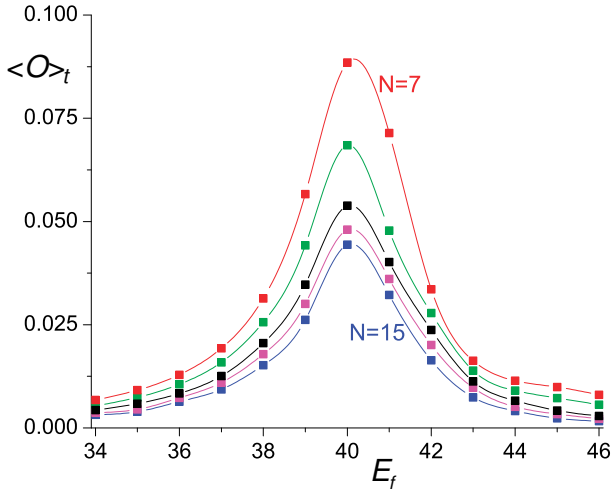

Fig. 1.6. Size dependence of the 'dynamic' results in Fig. 1.5. The sizes range from $N = 7$ to $N = 15$ (as labeled), with the intermediate values $N = 9, 11, 13$: $\langle O\rangle_t$ decreases monotonically with N.

Figure 1.3 shows the oscillations of the order parameter $O(t)$ for different values of E_f for $N = 13$. In agreement with our qualitative expectations, the oscillations have maximum amplitude when $E_f/t \approx 40$ is near the critical value $E_c/t = 41.85$. For either $E_f \ll E_c$ or $E_f \gg E_c$, the oscillations have a small amplitude around $O(t = 0)$. Furthermore, it is only for $E_f \approx E_c$ that the time averaged value of $O(t)$ is appreciable. Figure 1.4 shows the system size dependence of the time evolution for $E_f = U = 40t$. We find that the oscillations remain visible as we go to higher system sizes, although they do weaken somewhat. More significantly, the time averaged value of $O(t)$ remains non-zero, and has a weaker decrease with system size. In Fig. 1.5, we plot the long-time limit of the Ising order parameter, $\langle O\rangle_t$, as a function of E_f, and compare it with $O_{\rm ad}$, the value of the order parameter when E reaches E_f adiabatically and the wave function is that of the ground state at $E = E_f$. We find that $\langle O\rangle_t$ stays close to $O_{\rm ad}$ as long as there is a large overlap between the old and the new ground states. However, as we approach the adiabatic phase transition point, this overlap decreases and $\langle O\rangle_t$ cannot follow $O_{\rm ad}$ any more. The deviation of $\langle O\rangle_t$ is therefore a signature that the system is now in a different phase for the new value of the electric field. The 'dynamic' curve in Fig. 1.5 shows that the Mott insulator has a resonantly strong response to an electric field $E \sim U$ induced by the proximity of a QCP.

We comment briefly on the nature of the thermodynamic limit, $N \to \infty$ for the results in Figs. 1.2 and 1.3. For $O_{\rm ad}$ it is clear that there is a non-zero limit only for $E > E_c$, when it equals the order parameter of the spontaneously broken Ising symmetry. If we assume that the system thermalizes at long times for the dynamic case, then $\langle O\rangle_t$ corresponds to the expectation value of the equilibrium order parameter in $H_{1D}[E_f]$ at some finite temperature. In one dimension, it is not possible to break a discrete symmetry at finite temperatures, and so the thermodynamic limit of the order parameter must always vanish. By this reasoning, we expect $\langle O\rangle_t$ to also vanish in the thermodynamic limit. This is consistent with the results in Fig. 1.6, where we show the N dependence of the long-time limit $\langle O\rangle_t$. Our data are at present not extensive enough to definitely characterize the dependence of $\langle O\rangle_t$ on N.

1.2.2 Infinite range Ising model in a transverse field

The analysis of the quench dynamics of 1D ultracold atoms do not permit an analytical description of the long-time value of the order parameter. In particular, the system size dependence of the peak height of $\langle O\rangle_t$ is not easy to understand analytically in this model. For this purpose, we now consider a simple model system, the infinite range ferromagnetic spin-1/2 Ising model in a transverse field, and study its quench dynamics due to a sudden variation of the transverse field. The model Hamiltonian is given by [8]

$$H \;=\; -\;\frac{J}{N}\sum_{i<j} S_i^z S_j^z \;-\; \Gamma\sum_i S_i^x\;, \tag{1.7}$$

where $S_i^a = \sigma_i^a/2$, $a = x,y,z$, denote the components of the spin-1/2 operator represented by the standard Pauli spin matrices σ^a. Here we assume that $J \geq 0$ (ferromagnetic Ising interaction). This Hamiltonian is invariant under the Z_2 symmetry

$S_i^x \to S_i^x$, $S_i^y \to -S_i^y$, and $S_i^z \to -S_i^z$. (The Z_2 symmetry would not be present if there was a longitudinal magnetic field coupling to $\sum_i S_i^z$). We take $\Gamma \geq 0$ without loss of generality since we can always resort to the unitary transformation $S_i^x \to -S_i^x$, $S_i^y \to -S_i^y$ and $S_i^z \to S_i^z$, which flips the sign of Γ but leaves J unchanged. Eq. (1.7) can be written as

$$H = -\frac{J}{2N}\,(\,S_{tot}^z\,)^2 \;-\; \Gamma\, S_{tot}^x\;, \tag{1.8}$$

$$\text{where}\quad S_{tot}^z = \sum_i S_i^z, \qquad S_{tot}^x = \sum_i S_i^x, \tag{1.9}$$

and we have dropped a constant $(J/2N)\sum_i (S_i^z)^2 = J/8$ from the Hamiltonian in Eq. (1.8). This model has been studied extensively, particularly from the point of view of quantum entanglement [18]. Note that this model differs from the one studied in Ref. [19], where the spins were taken to be living on two sub-lattices, with Ising interactions only between spins on different sub-lattices.

We begin with a mean field analysis of the thermodynamics of the model described by Eq. (1.7). Denoting the mean field value $m = \sum_i \langle S_i^z \rangle / N$, the Hamiltonian governing any one of the spins is given by

$$h \;=\; -Jm S_{tot}^z \;-\; \Gamma S_{tot}^x\;. \tag{1.10}$$

This is a two-state problem whose partition function can be found at any temperature T. If $\beta = 1/(k_B T)$, we find that m must satisfy the self-consistent equation

$$m \;=\; \frac{Jm}{2\sqrt{\Gamma^2 + J^2 m^2}}\,\tanh\left(\frac{\beta\sqrt{\Gamma^2 + J^2 m^2}}{2}\right)\;. \tag{1.11}$$

This always has the trivial solution $m = 0$. In the limit of zero temperature, there is a non-trivial solution if $\Gamma < J/2$, with $|m| = (1/2)\sqrt{1 - 4\Gamma^2/J^2}$; the energy gap in that case is given by $J/2$. If $\Gamma > J/2$, we have $m = 0$ and the gap is given by $\Gamma - J/2$. Hence there is a zero temperature phase transition at $\Gamma_c = J/2$. The Z_2 symmetry mentioned after Eq. (1.7) is spontaneously broken and $< S_i^z >$ becomes non-zero when one crosses from the paramagnetic phase at $\Gamma > J/2$ into the ferromagnetic phase $\Gamma < J/2$.

In the plane of $(k_B T/J, \Gamma/J)$, there is a ferromagnetic (FM) region in which the solution with $m \neq 0$ has a lower free energy (the Z_2 symmetry is broken), and a paramagnetic (PM) region in which $m = 0$. The boundary between the two is obtained by taking the limit $m \to 0$ in (1.11). This gives $2\Gamma/J = \tanh(\beta\Gamma/2)$, i.e.,

$$\frac{k_B T}{J} \;=\; \frac{\Gamma}{J}\;\left[\ln\left(\frac{1 + 2\Gamma/J}{1 - 2\Gamma/J}\right)\right]^{-1}. \tag{1.12}$$

The mean-field phase diagram is shown in Fig. 1.7. We note that the exact excitation spectrum of this model can also be obtained analytically [8].

Having obtained the phase diagram, we now study the quench dynamics across the QCP. To begin with, we study the dynamics of the equal-time order parameter

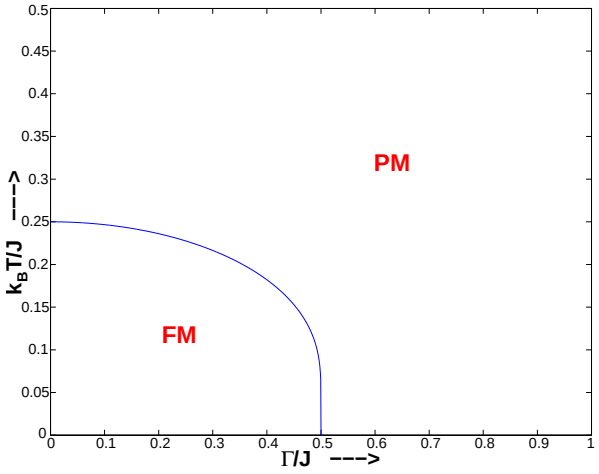

Fig. 1.7. Phase diagram of the model in mean field theory. FM and PM denote ferromagnetic and paramagnetic regions respectively.

correlation function (EOC) (defined as $\left\langle (S^z_{tot})^2 \right\rangle / S^2$) by changing the transverse field Γ from an initial value $\Gamma_i \gg \Gamma_c$ to a final value Γ_f suddenly, so that the ground state of the system has no time to change during the quench. In this case, just after the quench, the ground state of the system can be expressed, in terms of the eigenstates $|n\rangle$ of the new Hamiltonian $\mathscr{H}_f = -(J/4S)(S^z_{tot})^2 - \Gamma_f S^x_{tot}$ as

$$|\psi\rangle = \sum_n c_n |n\rangle , \tag{1.13}$$

where c_n denotes the overlap of the eigenstate $|n\rangle$ with the old ground state $|\psi\rangle$. As the state of the system evolves, it is given at time t by

$$|\psi(t)\rangle = \sum_n c_n e^{-iE_n t} |n\rangle , \tag{1.14}$$

where $E_n = \langle n| \mathscr{H}_f |n\rangle$ are the energy eigenvalues of the Hamiltonian $\mathscr{H}_f$. The EOC can thus be written as

$$\langle \psi(t)| (S^z_{tot})^2/S^2 |\psi(t)\rangle \;=\; \sum_{m,n} c_n c_m \, \cos\left[(E_n - E_m)\, t\right] \; \langle m| (S^z_{tot})^2/S^2 |n\rangle . \tag{1.15}$$

Eq. (1.15) can be solved numerically to obtain the time evolution of the EOC. We note that, similar to the case of the dipole model discussed in Sect. 1.2.1, we expect the amplitude of oscillations to be maximum when Γ_f is near Γ_c. This is verified in Fig. 1.8. Here, we have quenched the transverse fields to $\Gamma_f/J = 0.9, 0.01,$ and 0.4 starting from $\Gamma_i/J = 2.0$. The oscillation amplitudes of the EOC for $S = 100$, as shown in Fig. 1.8, are small for $\Gamma_f = 0.9$ and 0.01, whereas it is substantially larger for $\Gamma_f = 0.4$.

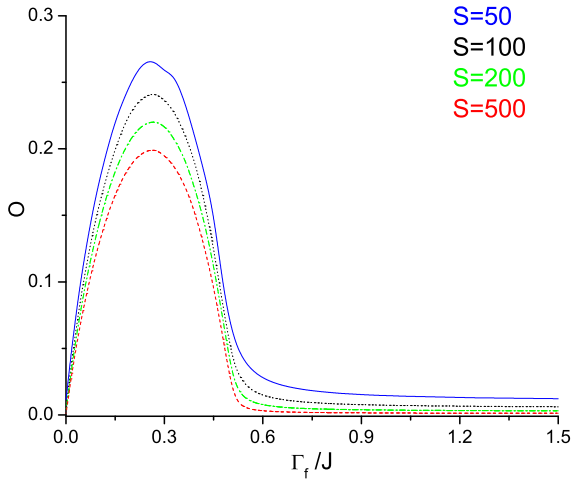

Fig. 1.8. Dynamics of $\left\langle (S^z_{tot})^2 \right\rangle / S^2$ for $S = 100$ after quenching the transverse field to different values Γ_f/J from an initial field $\Gamma_i/J = 2$. The oscillation amplitudes are small, as seen from the solid (red) and dotted (blue) curves corresponding to $\Gamma_f/J = 0.9$ and 0.01 respectively, far away from the critical point $\Gamma_c/J = 0.5$. The oscillation is large in the ordered phase near the critical point as seen from the dashed (black) curve $\Gamma_f/J = 0.4$.

Next, to understand the dynamics of the EOC in a little more detail, we study its long-time averaged value given by

$$\begin{aligned} O &= \lim_{T\to\infty} \left\langle \left\langle (S^z_{tot})^2(t) \right\rangle \right\rangle_T / S^2 \\ &= \frac{1}{S^2} \sum_n c_n^2 \langle n | (S^z_{tot})^2 | n \rangle \end{aligned} \tag{1.16}$$

for different Γ_f. Note that the long-time average depends on the product of the overlap of the state $|n\rangle$ with the old ground state and the expectation of $(S^z_{tot})^2$ in that state. From our earlier discussion in Sect. 1.2.1, we therefore expect O to have a peak somewhere near the critical point where such an overlap is maximized. This is verified by explicit numerical computation of Eq. (1.16) in Fig. 1.9 for several values of S and $\Gamma_i/J = 2$. We find that O peaks around $\Gamma_f/J = 0.25$, and the peak height decreases slowly with increasing S.

To understand the position and the system size dependence of the peak in O, we now look at the thermodynamic (large system size) limit; in the present model, this is also the large S and therefore classical limit. With this observation, we study the classical equations of motion for $\mathbf{S} = S(\cos\phi \sin\theta, \sin\phi \sin\theta, \cos\theta)$ for $\Gamma = \Gamma_f$. In the present model, S is a constant. Thus in the classical limit, we need to study the equations of motion for θ and ϕ. To this end, we note that the classical Lagrangian can be written in terms of θ and ϕ as [20]

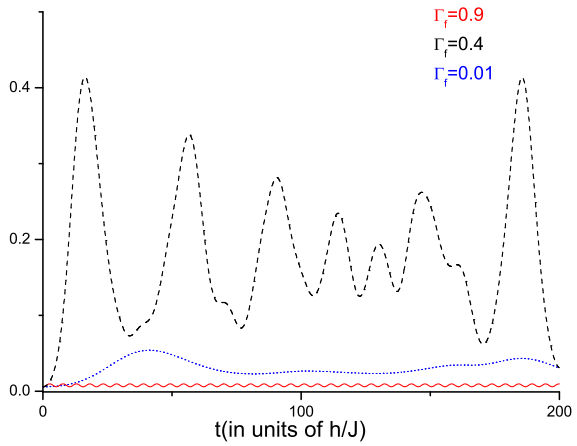

Fig. 1.9. Plot of the long-time average O as a function of Γ_f/J for different S. The solid (blue), dotted (black), dash-dotted (green) and the dashed (red) lines represent respectively the results for $S = 50$, $S = 100$, $S = 200$ and $S = 500$. O peaks around $\Gamma_f/J = 0.25$, and the peak value decreases with increasing S. We have chosen $\Gamma_i/J = 2$ for all the plots.

$$L = -S\,[1-\cos\theta]\,\frac{d\phi}{dt} \;-\; \mathscr{H}\,[\theta,\phi]\,. \tag{1.17}$$

This gives the equations of motion

$$\begin{aligned}\frac{d\theta}{dt} &= \Gamma_f\,\sin\phi\;,\\ \frac{d\phi}{dt} &= -\,\frac{J}{2}\,\cos\theta \;+\; \Gamma_f\,\cot\theta\cos\phi\;.\end{aligned} \tag{1.18}$$

Eq. (1.18) has to be supplemented with the initial condition that $S^x_{tot} = S$ at $t = 0$. The condition $S^x_{tot} = S$ corresponds to $\theta = \pi/2$, $\phi = 0$ which is also a fixed point of (1.18). Therefore we shall start from an initial condition which is very close to the fixed point: $\theta = \pi/2 - \varepsilon$, $\phi = \varepsilon$, where ε is an arbitrarily small constant. Further, since the motion occurs on a constant energy surface after the quench has taken place, we have

$$\Gamma_f = \frac{J}{4}\,\cos^2\theta \;+\; \Gamma_f\,\sin\theta\cos\phi\;. \tag{1.19}$$

Using (1.18) and (1.19), we get an equation of motion for θ in closed form,

$$\frac{d\theta}{dt} = \frac{\sqrt{\Gamma_f^2\sin^2(\theta) - \left[\Gamma_f - \frac{J}{4}\cos^2\theta\right]^2}}{\sin\theta} \equiv f(\theta)\,. \tag{1.20}$$

It can be seen that the motion of θ is oscillatory and has classical turning points at $\theta_1 = \sin^{-1}\left(\left|1-4\Gamma_f/J\right|\right)$ and $\theta_2 = \pi/2$. One can now obtain $\left\langle (S^z_{tot})^2\right\rangle_T = \left\langle \cos^2\theta\right\rangle_T$

from (1.20),

$$\left\langle \cos^2\theta \right\rangle_T = \mathscr{N}/\mathscr{D}\,, \tag{1.21}$$

$$\text{where} \quad \mathscr{N} = \int_{\theta_1}^{\theta_2} d\theta\, \frac{\cos^2\theta}{f(\theta)} \;=\; 4\sqrt{8\Gamma_f\left(J-2\Gamma_f\right)}/J\,, \tag{1.22}$$

$$\text{and} \quad \mathscr{D} = \int_{\theta_1}^{\theta_2} d\theta\, \frac{1}{f(\theta)}\,. \tag{1.23}$$

When trying to evaluate $\mathscr{D}$, we find that the integral has an end-point singularity at θ_2; this can be regulated by a cut-off η so that $\theta_2 = \pi/2 - \eta$. With this regularization, $\mathscr{D} = -J\ln(\eta)/\sqrt{\Gamma_f\left(J-2\Gamma_f\right)/2}$. The cut-off used here has a physical meaning and is not arbitrary. To see this, note that the angles (θ,ϕ) define the surface of a unit sphere of area 4π. This surface, for a system with spin S, is also the phase space which has $2S+1$ quantum mechanical states. For large S, the area of the surface occupied by each quantum mechanical state is therefore $4\pi/(2S+1) \simeq 2\pi/S$. In other words, each quantum mechanical state will have a linear dimension of order $1/\sqrt{S}$; this is how close we can get to a given point on the surface of the sphere. Note that this closeness is determined purely by quantum fluctuation and vanishes for $S \to \infty$. Thus η, which is also a measure of how close to the point $\theta = \pi/2$ we can get, must be of the order of $1/\sqrt{S}$; this determines the system-size dependence of $\left\langle \cos^2\theta \right\rangle_T$. Using (1.21), we finally get

$$\left\langle \cos^2\theta \right\rangle_T = \frac{16\Gamma_f\left(J-2\Gamma_f\right)}{J^2\ln(S)}. \tag{1.24}$$

Eq. (1.24) is one of the main results of this section. It demonstrates that the long-time average of the EOC must be peaked at $\Gamma_f/J = 0.25$ which agrees perfectly with the exact quantum mechanical numerical analysis leading to Fig. 1.9. Moreover, it provides an analytical understanding of the S (and hence system size) dependence of the peak values of Γ_f/J; we conclude that the peak in O vanishes logarithmically with the system size S. Such a slow variation with S shows that it might be experimentally possible to observe an experimental signature of a QCP for a possible realization of this model with ultracold atoms where $N \sim 10^5 - 10^6$ [8].

The results obtained in this section can be tested in two kinds of experimental systems. One class of systems are those with long-range dipole-dipole interactions such as KH_2PO_4 or $Dy(C_2H_5SO_4)_3 9H_2O$ [21] which exhibit order-disorder transitions driven by tunneling fields. The other class of systems are two-component Bose-Einstein condensates where the inter-species interaction is strong compared to the intra-species interaction; the relative strengths of these interactions can be changed by tuning the system to be near a Feshbach resonance as discussed for the $^{41}K-^{87}Rb$ system in Refs. [22, 23, 24, 25]. The quench dynamics that we have discussed can be realized by applying a radio frequency pulse to the system and suddenly changing the frequency of the pulse.

We end this section with the observation that the resonant response of the order parameter during quench dynamics has been found in two very disparate models

(1D ultracold atoms and infinite dimensional Ising ferromagnet) and therefore seems to be a universal signature of the QCP through which the system passes during its evolution.

1.3 Non-adiabatic dynamics

In recent years, there have been extensive studies of what happens when a parameter λ in the Hamiltonian of a quantum system is varied in time slowly (non-adiabatically) so as to take the system through a QCP. A quantum phase transition is necessarily accompanied by diverging length and and time scales, or, equivalently, a vanishing energy gap between the ground state and the first excited state [1]. A consequence of this is that the system fails to be in the adiabatic limit when it crosses a critical point. Namely, when λ is varied across the QCP located at $\lambda = \lambda_c$ at a finite rate given by $1/\tau$ (where τ will be called the quench time), the system fails to follow the instantaneous ground state in a finite region around λ_c. As a result, defects are produced [10, 26]. For a slow quench (for instance, for values of τ much larger than the inverse band width) which takes the system across a QCP in a linear way, it is well-known that the density of defects n scales as a power of the quench time, $n \sim 1/\tau^{d\nu/(z\nu+1)}$, where ν and z are respectively the correlation length and the dynamical critical exponents characterizing the critical point [12, 27]. A theoretical study of a quench dynamics requires a knowledge of the excited states of the system. Hence, early studies of the quench problem were mostly restricted to quantum phase transitions in exactly solvable models such as the 1D Ising model in a transverse field [4, 28, 29], the 1D XY spin-1/2 model [30, 33], quantum spin chains [31, 32, 34], the Bose-Hubbard model [35], the Falicov-Kimball model [36] and 1D spinless fermionic chains [37]. Experimentally, trapped ultracold atoms in optical lattices provide possibilities of realization of many of the above-mentioned systems [38, 39]. Experimental studies of defect production due to quenching of the magnetic field in a spin-1 Bose condensate have also been undertaken [40].

A class of models in which the above power law scaling can be derived easily is one in which, due to the existence of a mapping to a system of non-interacting fermions, the system decomposes into a product of two-level systems. For instance, this occurs in the 1D XY spin-1/2 model and in the two-dimensional (2D) spin-1/2 Kitaev model. In both these cases, it turns out that the Hamiltonian is given by a sum of terms of the form

$$H_{\mathbf{k}} = \alpha(\mathbf{k})(c_{\mathbf{k}}^{\dagger}c_{\mathbf{k}} + c_{-\mathbf{k}}^{\dagger}c_{\mathbf{k}}) + \Delta^{*}(\mathbf{k})c_{\mathbf{k}}^{\dagger}c_{-\mathbf{k}}^{\dagger} + \Delta(\mathbf{k})c_{-\mathbf{k}}c_{\mathbf{k}}, \tag{1.25}$$

where $\mathbf{k}$ runs over *half* the Brillouin zone (BZ), and $\alpha(\mathbf{k})$ is real. This Hamiltonian acts on a space spanned by four states, namely, the empty state $|0\rangle$, two one-fermion states $c_{\mathbf{k}}^{\dagger}|0\rangle = |\mathbf{k}\rangle$ and $c_{-\mathbf{k}}^{\dagger}|0\rangle = |-\mathbf{k}\rangle$, and a two-fermion state $c_{\mathbf{k}}^{\dagger}c_{-\mathbf{k}}^{\dagger}|0\rangle = |\mathbf{k},-\mathbf{k}\rangle$. Both the one-particle states are eigenstates of $H_{\mathbf{k}}$ with the same eigenvalue $\alpha(\mathbf{k})$. On the other hand, the states $|0\rangle$ and $|\mathbf{k},-\mathbf{k}\rangle$ are governed by a 2×2 Hamiltonian given by

$$h_{\mathbf{k}} \;=\; \begin{pmatrix} 0 & \Delta(\mathbf{k}) \\ \Delta^*(\mathbf{k}) & 2\alpha(\mathbf{k}) \end{pmatrix}. \tag{1.26}$$

The eigenvalues of this are given by $\alpha(\mathbf{k}) \pm \sqrt{\alpha^2(\mathbf{k}) + |\Delta(\mathbf{k})|^2}$; since the lower eigenvalue is less than $\alpha(\mathbf{k})$, the ground state lies within the subspace of the states $|0\rangle$ and $|\mathbf{k}, -\mathbf{k}\rangle$. We observe that the Hamiltonian in (1.25) does not mix the states $|0\rangle$ and $|\mathbf{k}, -\mathbf{k}\rangle$ with the states $|\mathbf{k}\rangle$ and $|-\mathbf{k}\rangle$, *even if* $\alpha(\mathbf{k})$ and $\Delta(\mathbf{k})$ change with time. Hence, if we start at time $t \to -\infty$ with a linear superposition of $|0\rangle$ and $|\mathbf{k}, -\mathbf{k}\rangle$, we will end at $t \to \infty$ with a superposition of the same two states. In that case, it is sufficient to restrict our attention to the Hamiltonian for a two-level system given in (1.26). We can rewrite that as

$$h_{\mathbf{k}} \;=\; \alpha(\mathbf{k})\, I_2 \;-\; \alpha(\mathbf{k})\, \sigma^3_{\mathbf{k}} \;+\; \Delta(\mathbf{k})\, \sigma^+_{\mathbf{k}} \;+\; \Delta^*(\mathbf{k})\, \sigma^-_{\mathbf{k}}, \tag{1.27}$$

where I_2 is the identity matrix, and σ^3 and $\sigma^{\pm} = (\sigma^1 \pm i\sigma^2)/2$ denote the Pauli matrices. We can ignore the term $\alpha(\mathbf{k})I_2$ in (1.27) since this only affects the wave function by a time-dependent phase factor.

Let us now consider what happens if $\alpha(\mathbf{k})$ varies linearly with time. Then the total Hamiltonian H_d for all the two-level systems can be written as

$$H_d \;=\; \sum_{\mathbf{k}} h_{\mathbf{k}}, \quad \text{where} \quad h_{\mathbf{k}} \;=\; \frac{t}{\tau}\, \varepsilon(\mathbf{k})\, \sigma^3_{\mathbf{k}} \;+\; \Delta(\mathbf{k})\, \sigma^+_{\mathbf{k}} \;+\; \Delta^*(\mathbf{k})\, \sigma^-_{\mathbf{k}}, \tag{1.28}$$

where d is the number of spatial dimensions, and the sum over $\mathbf{k}$ runs over half the BZ. If $\varepsilon(\mathbf{k}) > 0$, the ground state is given by $|0\rangle$ as $t \to -\infty$ and by $|\mathbf{k}, -\mathbf{k}\rangle$ as $t \to \infty$. If we begin with the state $|0\rangle$ at $t = -\infty$ and evolve the system using the time-dependent Schrödinger equation, we end at $t = \infty$ in a state which is a superposition of states $|0\rangle$ and $|\mathbf{k}, -\mathbf{k}\rangle$ with probabilities $p_{\mathbf{k}}$ and $1 - p_{\mathbf{k}}$, where $p_{\mathbf{k}}$ is given by the Landau-Zener expression [41]

$$p_{\mathbf{k}} \;=\; e^{-\pi\tau|\Delta(\mathbf{k})|^2/\varepsilon(\mathbf{k})}. \tag{1.29}$$

Note that $p_{\mathbf{k}} \to 1$ for $\tau \to 0$ (sudden quench) and $\to 0$ for $\tau \to \infty$ (adiabatic quench), as expected. Let us now assume that the gap function $\Delta(\mathbf{k})$ vanishes at some point $\mathbf{k}_0$ in the BZ as $|\Delta(\mathbf{k})| \simeq a_0|\mathbf{k} - \mathbf{k}_0|^z$, while $\varepsilon(\mathbf{k}_0) = b_0$ is finite; this corresponds to a QCP with an arbitrary value of z, but with $z\nu = 1$. The density of defects n in the final state is given by the density of fermions $n = \int d^d\mathbf{k} p_{\mathbf{k}}$. In the adiabatic limit $\tau \to \infty$, this is given by

$$\int_{\mathbf{k}\sim\mathbf{k}_0} d^d k\, e^{-\pi\tau a_0^2|\mathbf{k}-\mathbf{k}_0|^{2z}/b_0} \;\sim\; 1/\tau^{d/(2z)}, \tag{1.30}$$

which is the expected result for $z\nu = 1$.

It is useful to note that the derivation of the scaling law in (1.30) does not require a knowledge of the precise functional form given in (1.29). It is enough to know that $p_{\mathbf{k}}$ must be a function of the form $f(\tau|\Delta(\mathbf{k})|^2/\varepsilon(\mathbf{k}))$, where $f(x) \to 1$ for $\tau \to 0$ and $\to 0$ for $\tau \to \infty$; these limiting values follow from general properties of the time-dependent Schrödinger equation. The argument of the function f can be derived by

considering the equation $i\partial\psi_{\mathbf{k}}(t)/\partial t = h_{\mathbf{k}}\psi_{\mathbf{k}}(t)$, performing a phase re-definition to change $\Delta(\mathbf{k})$ to $|\Delta(\mathbf{k})|$, multiplying both sides by $\sqrt{\tau/\varepsilon(\mathbf{k})}$ and rescaling t to $t\sqrt{\tau/\varepsilon(\mathbf{k})}$. This effectively converts $h_{\mathbf{k}}$ to the form $t\sigma_{\mathbf{k}}^3 + |\Delta(\mathbf{k})|\sqrt{\tau/\varepsilon(\mathbf{k})}(\sigma_{\mathbf{k}}^+ + \sigma_{\mathbf{k}}^-)$; hence the probability $p_{\mathbf{k}}$ of starting in the ground state $\begin{pmatrix}1\\0\end{pmatrix}$ at $t=-\infty$ and ending in the same state (which is the excited state) at $t=\infty$ must be a function of $\tau|\Delta(\mathbf{k})|^2/\varepsilon(\mathbf{k})$.

We can generalize the above results to a QCP with arbitrary values of z and ν. We consider a generic time-dependent Hamiltonian $H(t) \equiv H[\lambda(t)]$, whose states are labeled by $|\mathbf{k}\rangle$, and $|0\rangle$ denotes the ground state. If there is a second order phase transition, the basis states change continuously with time during this evolution and can be written as $|\psi(t)\rangle = \sum_{\mathbf{k}} a_{\mathbf{k}}(t)|\mathbf{k}[\lambda(t)]\rangle$. The defect density can be obtained in terms of the coefficients $a_{\mathbf{k}}(t)$ as $n = \sum_{\mathbf{k}\neq 0}|a_{\mathbf{k}}(t\to\infty)|^2$; hence one gets [12]

$$n \sim \int d^dk \left| \int_{-\infty}^{\infty} d\lambda \, \langle \mathbf{k}|\frac{d}{d\lambda}|0\rangle \, e^{i\tau\int^{\lambda} d\lambda' \delta\omega_{\mathbf{k}}(\lambda')}\right|^2, \tag{1.31}$$

where $\delta\omega_{\mathbf{k}}(\lambda) = \omega_{\mathbf{k}}(\lambda) - \omega_0(\lambda)$ are the instantaneous excitation energies. Following Ref. [12], we note that near a QCP, $\delta\omega_{\mathbf{k}}(\lambda) = \Delta F(\Delta/|\mathbf{k}|^z)$, where Δ is the energy gap, z is the dynamical critical exponent and $F(x) \sim 1/x$ for large x; we have assumed here that the gap vanishes as $\mathbf{k}=\mathbf{0}$. Also, since the quench term vanishes at the critical point as $\Delta \sim |\lambda|^{z\nu}$, one can write $\delta\omega_{\mathbf{k}}(\lambda) = |\lambda|^{z\nu}\tilde{F}(|\lambda|^{z\nu}/|\mathbf{k}|^z)$ where $\tilde{F}(x) \sim 1/x$ for large x. Further, one has $\langle\mathbf{k}|\frac{d}{d\Delta}|0\rangle = |\mathbf{k}|^{-z}G(\Delta/|\mathbf{k}|^z)$ near a critical point where $G(0)$ is a constant. This allows us to write $\langle\mathbf{k}|\frac{d}{d\lambda}|0\rangle = \lambda^{z\nu-1}|\mathbf{k}|^{-z}G'(\lambda^{z\nu}/|\mathbf{k}|^z)$ where $G'(0)$ is a constant [1, 12]. Substituting these in (1.31) and changing the integration variables to $\eta = \tau^{\nu/(z\nu+1)}|\mathbf{k}|$ and $\xi = |\mathbf{k}|^{-1/\nu}\lambda$, we find that

$$n \sim \tau^{-d\nu/(z\nu+1)}. \tag{1.32}$$

We will now discuss two major extensions of the above results: (i) what happens if the system is taken across a $d-m$ dimensional quantum critical surface instead of a QCP [13], and (ii) what happens if the quenching across a QCP is non-linear in time [14, 42]. We will show that in both cases, the defect density still scales as a power of the quench time, but the power is not equal to the universal value $d\nu/(z\nu+1)$ mentioned above; rather it depends on other parameters such as m or the degree of non-linearity.

1.3.1 Quenching across a critical surface

When a quench takes a quantum system across a critical surface rather than a critical point, the density of defects scales in a different way with the quench time. To give a simple argument, consider a d-dimensional model with $z=\nu=1$ which is described by the Hamiltonian given in (1.28). Suppose that a quench takes the system through a critical surface of $d-m$ dimensions. The defect density for a sufficiently slow quench is then given by [41] $n \sim \int_{\mathrm{BZ}} d^dk e^{-\pi\tau f(\mathbf{k})}$, where $f(\mathbf{k}) = |\Delta(\mathbf{k})|^2/|\varepsilon(\mathbf{k})|$ vanishes on the $d-m$ dimensional critical surface. We can then write

$$n \sim \int_{\rm BZ} d^d k \, \exp[-\pi\tau \sum_{\alpha,\beta=1}^{m} g_{\alpha\beta} k_\alpha k_\beta] \sim 1/\tau^{m/2}, \tag{1.33}$$

where α, β denote one of the m directions orthogonal to the critical surface, and $g_{\alpha\beta} = [\partial^2 f(\mathbf{k})/\partial k_\alpha \partial k_\beta]_{\mathbf{k} \in \text{critical surface}}$. Note that this result depends only on the property that $f(\mathbf{k})$ vanishes on a $d-m$ dimensional surface, and not on the precise form of $f(\mathbf{k})$. For general values of z and ν, we note that the Landau-Zener type of scaling argument yields $\Delta \sim 1/\tau^{d\nu/(z\nu+1)}$, where Δ is the energy gap [12]. When one crosses a $d-m$ dimensional critical surface during the quench, the available phase space Ω for defect production scales as $\Omega \sim k^m \sim \Delta^{m/z} \sim 1/\tau^{m\nu/(z\nu+1)}$; this leads to $n \sim 1/\tau^{m\nu/(z\nu+1)}$. For a quench through a critical point where $m = d$, we retrieve the results of Ref. [12].

To give an example of a quench across a critical line, let us consider a model which was proposed recently by Kitaev. This is a 2D spin-1/2 model on a honeycomb lattice as shown in Fig. 1.10; the Hamiltonian is given by [46]

$$H_K = \sum_{j+l=\text{even}} (J_1 \sigma^x_{j,l} \sigma^x_{j+1,l} + J_2 \sigma^y_{j-1,l} \sigma^y_{j,l} + J_3 \sigma^z_{j,l} \sigma^z_{j,l+1}), \tag{1.34}$$

where j and l denote the column and row indices of the honeycomb lattice. This model has been studied extensively and it exhibits several interesting features [47, 48, 49, 50, 51, 52]. It provides a rare example of a 2D model which can be exactly solved using a Jordan-Wigner transformation [46, 47, 51, 52]. It has been shown in Ref. [46] that the presence of magnetic field, which induces a gap in the 2D gapless phase, leads to non-Abelian statistics of the low-lying excitations of the model; these excitations can be viewed as robust qubits in a quantum computer [53].

The Jordan-Wigner transformation of the Kitaev model to a model of non-interacting fermions works as follows. One can write

$$\begin{aligned} a_{jl} &= \left(\prod_{i=-\infty}^{j-1} \sigma^z_{il} \right) \sigma^y_{jl} \ \text{ for even } j+l, \\ b_{jl} &= \left(\prod_{i=-\infty}^{j-1} \sigma^z_{il} \right) \sigma^x_{jl} \ \text{ for odd } j+l. \end{aligned} \tag{1.35}$$

where the a_{jl} and b_{jl} are Majorana fermion operators (and hence Hermitian) obeying the anticommutation relations $\{a_{jl}, a_{j'l'}\} = \{b_{jl}, b_{j'l'}\} = \delta_{jj'}\delta_{ll'}$. This transformation maps the spin Hamiltonian in (1.34) to a fermionic Hamiltonian given by

$$H_K = i \sum_{\mathbf{n}} [J_1 \, b_{\mathbf{n}} a_{\mathbf{n}-\mathbf{M}_1} + J_2 \, b_{\mathbf{n}} a_{\mathbf{n}+\mathbf{M}_2} + J_3 D_{\mathbf{n}} \, b_{\mathbf{n}} a_{\mathbf{n}}], \tag{1.36}$$

where $\mathbf{n} = \sqrt{3}\hat{i}\, n_1 + (\frac{\sqrt{3}}{2}\hat{i} + \frac{3}{2}\hat{j})\, n_2$ denote the midpoints of the vertical bonds. Here n_1, n_2 run over all integers so that the vectors $\mathbf{n}$ form a triangular lattice whose vertices lie at the centers of the vertical bonds of the underlying honeycomb lattice; the Majorana fermions $a_{\mathbf{n}}$ and $b_{\mathbf{n}}$ sit at the top and bottom sites respectively of the bond

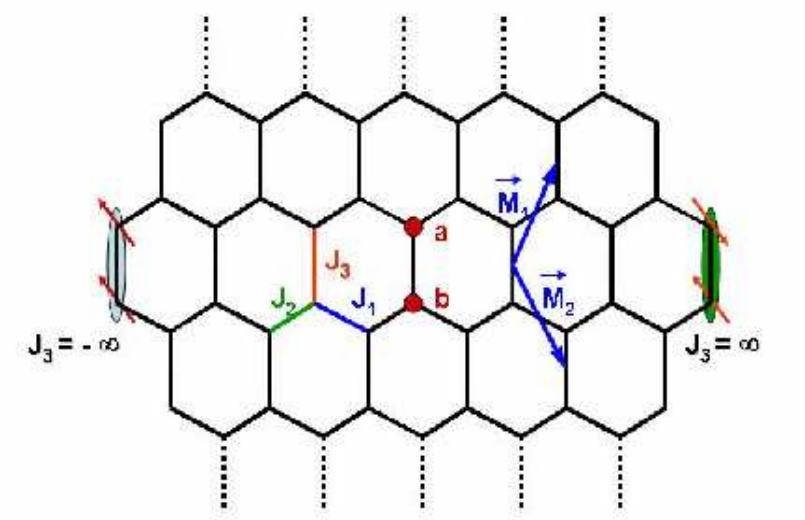

Fig. 1.10. Schematic representation of the Kitaev model on a honeycomb lattice showing the bonds J_1, J_2 and J_3. Schematic pictures of the ground states, which correspond to pairs of spins on vertical bonds locked parallel (antiparallel) to each other in the limit of large negative (positive) J_3, are shown at one bond on the left (right) edge respectively. $\mathbf{M}_1$ and $\mathbf{M}_2$ are spanning vectors of the lattice, and a and b represent inequivalent sites.

labeled $\mathbf{n}$. The vectors $\mathbf{M}_1 = \frac{\sqrt{3}}{2}\hat{i} + \frac{3}{2}\hat{j}$ and $\mathbf{M}_2 = \frac{\sqrt{3}}{2}\hat{i} - \frac{3}{2}\hat{j}$ are spanning vectors for the reciprocal lattice, and $D_{\mathbf{n}}$ can take the values ± 1 independently for each $\mathbf{n}$. The crucial point that makes the solution of Kitaev model feasible is that $D_{\mathbf{n}}$ commutes with H_K, so that all the eigenstates of H_K can be labeled by a specific set of values of $D_{\mathbf{n}}$. It has been shown that for any value of the parameters J_i, the ground state of the model always corresponds to $D_{\mathbf{n}} = 1$ on all the bonds. Since $D_{\mathbf{n}}$ is a constant of motion, the dynamics of the model starting from any ground state never takes the system outside the manifold of states with $D_{\mathbf{n}} = 1$.

For $D_{\mathbf{n}} = 1$, it is straightforward to diagonalize H_K in momentum space. We define Fourier transforms of the Majorana operators $a_{\mathbf{n}}$ as

$$a_{\mathbf{n}} = \sqrt{\frac{4}{N}} \sum_{\mathbf{k}} [\, a_{\mathbf{k}}\, e^{i\mathbf{k}\cdot\mathbf{n}} + a_{\mathbf{k}}^{\dagger}\, e^{-i\mathbf{k}\cdot\mathbf{n}} \,],$$
$$b_{\mathbf{n}} = \sqrt{\frac{4}{N}} \sum_{\mathbf{k}} [\, b_{\mathbf{k}}\, e^{i\mathbf{k}\cdot\mathbf{n}} + b_{\mathbf{k}}^{\dagger}\, e^{-i\mathbf{k}\cdot\mathbf{n}} \,], \tag{1.37}$$

where N is the number of sites (assumed to be even, so that the number of unit cells $N/2$ is an integer), and the sum over $\mathbf{k}$ extends over half the Brillouin zone of the honeycomb lattice. We have the anticommutation relations $\{a_{\mathbf{k}}, a_{\mathbf{k}'}^{\dagger}\} = \delta_{\mathbf{k},\mathbf{k}'}$, $\{a_{\mathbf{k}}, a_{\mathbf{k}'}\} = 0$, and similarly for $b_{\mathbf{k}}$ and $b_{\mathbf{k}}^{\dagger}$. We then obtain $H_K = \sum_{\mathbf{k}} \psi_{\mathbf{k}}^{\dagger} h_{\mathbf{k}} \psi_{\mathbf{k}}$, where $\psi_{\mathbf{k}}^{\dagger} = (a_{\mathbf{k}}^{\dagger}, b_{\mathbf{k}}^{\dagger})$, and $h_{\mathbf{k}}$ can be expressed in terms of Pauli matrices $\sigma^{1,2,3}$ as

$$h_{\mathbf{k}} = 2\,[J_1 \sin(\mathbf{k}\cdot\mathbf{M}_1) \;-\; J_2 \sin(\mathbf{k}\cdot\mathbf{M}_2)]\;\sigma^1 + 2\,[J_3 \;+\; J_1\cos(\mathbf{k}\cdot\mathbf{M}_1) \;+\; J_2\cos(\mathbf{k}\cdot\mathbf{M}_2)]\;\sigma^2. \tag{1.38}$$

The energy spectrum of H_K consists of two bands with energies

$$E^{\pm}_{\mathbf{k}} = \pm\,2\,[(J_1\sin(\mathbf{k}\cdot\mathbf{M}_1) - J_2\sin(\mathbf{k}\cdot\mathbf{M}_2))^2 + (J_3 + J_1\cos(\mathbf{k}\cdot\mathbf{M}_1) + J_2\cos(\mathbf{k}\cdot\mathbf{M}_2))^2]^{1/2}. \tag{1.39}$$

We note that for $|J_1 - J_2| \leq J_3 \leq J_1 + J_2$, these bands touch each other so that the energy gap $\Delta_{\mathbf{k}} = E^+_{\mathbf{k}} - E^-_{\mathbf{k}}$ vanishes for special values of $\mathbf{k}$ leading to a gapless phase of the model [46, 47, 49, 51].

We will now quench $J_3(t) = Jt/\tau$ at a fixed rate $1/\tau$, from $-\infty$ to ∞, keeping J, J_1 and J_2 fixed at some non-zero values; we have introduced the quantity J to fix the scale of energy. We note that the ground states of H_K corresponding to $J_3 \to -\infty(\infty)$ are gapped and have $\sigma^z_{j,l}\sigma^z_{j,l+1} = 1(-1)$ for all lattice sites (j,l). To study the state of the system after the quench, we first note that after an unitary transformation $U = \exp(-i\sigma_1\pi/4)$, one can write $H_K = \sum_{\mathbf{k}} \psi'^{\dagger}_{\mathbf{k}} h'_{\mathbf{k}} \psi'_{\mathbf{k}}$, where $h'_{\mathbf{k}} = U h_{\mathbf{k}} U^{\dagger}$ is given by

$$h'_{\mathbf{k}} = 2\,[J_1 \sin(\mathbf{k}\cdot\mathbf{M}_1) \;-\; J_2 \sin(\mathbf{k}\cdot\mathbf{M}_2)]\;\sigma^1 + 2\,[J_3(t) + J_1\cos(\mathbf{k}\cdot\mathbf{M}_1) + J_2\cos(\mathbf{k}\cdot\mathbf{M}_2)]\;\sigma^3. \tag{1.40}$$

Hence the off-diagonal elements of $h'_{\mathbf{k}}$ remain time-independent, and the problem of quench dynamics reduces to a Landau-Zener problem for each $\mathbf{k}$. The defect density can then be computed following a standard prescription [41]

$$n = \frac{1}{A}\int_{\mathbf{k}} d^2\mathbf{k}\; p_{\mathbf{k}}, \qquad p_{\mathbf{k}} = e^{-2\pi\tau\,[J_1\sin(\mathbf{k}\cdot\mathbf{M}_1) - J_2\sin(\mathbf{k}\cdot\mathbf{M}_2)]^2/J}, \tag{1.41}$$

where $A = 4\pi^2/(3\sqrt{3})$ denotes the area of half the Brillouin zone over which the integration is carried out. Since the integrand in (1.41) is an even function of $\mathbf{k}$, one can extend the region of integration over the full Brillouin zone. This region can be chosen to be a rhombus with vertices lying at $(k_x, k_y) = (\pm 2\pi/\sqrt{3}, 0)$ and $(0, \pm 2\pi/3)$. Introducing two independent integration variable v_1, v_2, each with a range $0 \leq v_1, v_2 \leq 1$, one finds that

$$k_x = 2\pi\,\frac{v_1 + v_2 - 1}{\sqrt{3}}, \quad k_y = 2\pi\,\frac{v_2 - v_1}{3}. \tag{1.42}$$

Such a substitution covers the rhombus uniformly and facilitates the numerical integration necessary for computing n.

A plot of n as a function of the quench time $J\tau$ and $\alpha = \tan^{-1}(J_2/J_1)$ (we have taken $J_{1[2]} = J\cos\alpha[\sin\alpha]$) is shown in Fig. 1.11. We note that the density of defects produced is maximum when $J_1 = J_2$. This is due to the fact that the length of the

gapless line through which the system passes during the quench is maximum at this point. This allows the system to remain in the non-adiabatic state for the maximum time during the quench, leading to the maximum density of defects. For $J_1/J_3 > 2J_2/J_3$, the system does not pass through a gapless phase during the quench, and the defect production is exponentially suppressed.

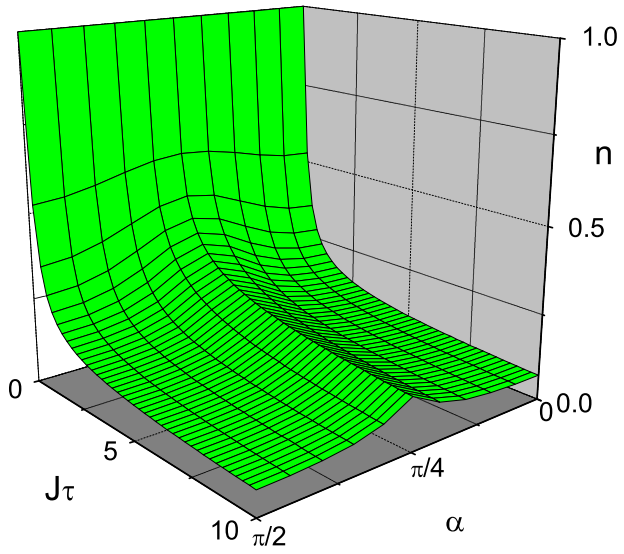

Fig. 1.11. Plot of defect density n as a function of the quench time $J\tau$ and $\alpha = \tan^{-1}(J_2/J_1)$. The density of defects is maximum at $J_1 = J_2$.

For sufficiently slow quench $2\pi J\tau \gg 1$, $p_{\mathbf{k}}$ is exponentially small for all values of $\mathbf{k}$ except in the region near the line

$$J_1 \sin(\mathbf{k}\cdot\mathbf{M}_1) - J_2 \sin(\mathbf{k}\cdot\mathbf{M}_2) = 0, \tag{1.43}$$

and the contribution to the momentum integral in (1.41) comes from values of $\mathbf{k}$ close to this line of zeroes. We note that the line of zeroes where $p_{\mathbf{k}} = 1$ precisely corresponds to the zeroes of the energy gap $\Delta_{\mathbf{k}}$ as J_3 is varied for a fixed J_2 and J_1. Thus the system becomes non-adiabatic when it passes through the intermediate gapless phase in the interval $|J_1 - J_2| \leq J_3(t) \leq J_1 + J_2$. It is then easy to see, by expanding $p_{\mathbf{k}}$ about this line that in the limit of slow quench, the defect density scales as $n \sim 1/\sqrt{\tau}$. We thus see that the scaling of the defect density with the quench rate when the system passes through a critical *line* in momentum space is different from the situation where the quench takes the system through a critical *point*. The Kitaev model is an example of a system in which $d = 2$, $m = 1$, and $z = \nu = 1$; this gives rise to a defect density scaling as $1/\sqrt{\tau}$.

Before ending this section, it is interesting to consider another aspect of the system after the quench. Since the time evolution of the system is unitary, it will al-

ways be in a pure state. However, for each value of k, the wave function is given by $\sqrt{1-p_{\mathbf{k}}}\psi_{2\mathbf{k}}e^{-iE_{2k}t} + \sqrt{p_{\mathbf{k}}}\psi_{1\mathbf{k}}e^{-iE_{1k}t}$, where E_{1k} (E_{2k}) $= \infty$ ($-\infty$). As a result, the final density matrix of the system will have off-diagonal terms involving $\psi^*_{2\mathbf{k}}\psi_{1\mathbf{k}}$ and $\psi^*_{1\mathbf{k}}\psi_{2\mathbf{k}}$ which vary extremely rapidly with time; their effects on physical quantities will therefore average to zero. Hence, for each momentum $\mathbf{k}$, the final density matrix $\rho_{\mathbf{k}}$ is effectively diagonal like that of a mixed state [30], where the diagonal entries are time-independent as $t \to \infty$ and are given by $1-p_k$ and p_k. Such a density matrix is associated with an entropy which we will now calculate. The density matrix of the entire system takes the product form $\rho = \bigotimes \rho_{\mathbf{k}}$. The von Neumann entropy density corresponding to this state is given by

$$s = -\frac{1}{A}\int d^2\mathbf{k}\,[\,(1-p_{\mathbf{k}})\ln(1-p_{\mathbf{k}}) + p_{\mathbf{k}}\ln p_{\mathbf{k}}\,], \tag{1.44}$$

where the integral again goes half the Brillouin zone. Let us now consider the dependence of this quantity on the quench time τ [33]. If τ is very small, the system stays in its initial state and $p_{\mathbf{k}}$ will be close to 1 for all values of $\mathbf{k}$; for the same reason, $\langle O_{\mathbf{0}}\rangle$ will remain close to 1. If τ is very large, the system makes a transition to the final ground state for all momentum except near the line described in (1.43). Hence $p_{\mathbf{k}}$ will be close to 0 for all $\mathbf{k}$ except near that line, and $\langle O_{\mathbf{0}}\rangle$ will be close to -1. In both these cases, the entropy density will be small. We therefore expect that there will be an intermediate region of values of τ in which s will show a maximum and $\langle O_{\mathbf{0}}\rangle$ will show a crossover from -1 to 1. A plot of s as a function of $J\tau$ and α shown in Fig. 1.12 confirms this expectation. We find that the entropy reaches a maximum for an intermediate value of $J\tau$ where $\langle O_{\mathbf{0}}\rangle$ crosses over from -1 to 1 for all values of α.

1.3.2 Non-linear quenching across a critical point

Let us now consider what happens if we start with a Hamiltonian similar to the one given in (1.28), except that

$$h_{\mathbf{k}}(t) = (\lambda(t)+b(\mathbf{k}))\sigma^3_{\mathbf{k}} + \Delta(\mathbf{k})\,\sigma^+_{\mathbf{k}} + \Delta^*(\mathbf{k})\,\sigma^-_{\mathbf{k}}, \tag{1.45}$$

where $\lambda(t) = \lambda_0|t/\tau|^\alpha \mathrm{sign}(t)$ is the quench parameter; $\alpha = 1$ corresponds to a linear quench. The instantaneous energies of the Hamiltonian in (1.45) are given by

$$E(\mathbf{k}) = \pm\sqrt{(\lambda(t)+b(\mathbf{k}))^2+|\Delta(\mathbf{k})|^2}. \tag{1.46}$$

These energy levels touch each other at $t = t_0$ and $\mathbf{k} = \mathbf{k}_0$, so that $|\Delta(\mathbf{k})| \sim |\mathbf{k}-\mathbf{k}_0|$ and $|t_0| = \tau|b(\mathbf{k}_0)/\lambda_0|^{1/\alpha} = \tau g^{1/\alpha}$, where $g = |b(\mathbf{k}_0)/\lambda_0|$ is a non-universal model-dependent parameter. At this point the energy levels cross and we have a QCP with $z = \nu = 1$. Note that the critical point is reached at $t = 0$ only if $b(\mathbf{k}_0)$ vanishes.

Let us first consider the case where $b(\mathbf{k}_0) = 0$ so that the system passes through the critical point at $t = 0$. In what follows, we shall assume that $|\Delta(\mathbf{k})| \sim |\mathbf{k}-\mathbf{k}_0|$ and $b(\mathbf{k}) \sim |\mathbf{k}-\mathbf{k}_0|^{z_1}$ at the critical point, where $z_1 \geq 1$ so that $E \sim |\mathbf{k}-\mathbf{k}_0|$ and $z = 1$.

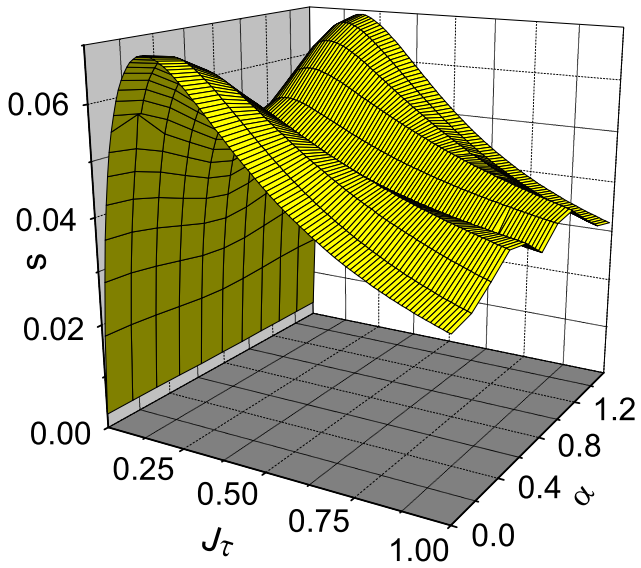

Fig. 1.12. Plot of the entropy density s as a function of $J\tau$ and $\alpha = \tan^{-1}(J_2/J_1)$. The entropy density peaks when $\langle O_{\mathbf{0}} \rangle$ crosses from -1 to 1.

In the rest of the analysis, we will scale $t \to t\lambda_0$, $\tau \to \tau\lambda_0$, $\Delta(\mathbf{k}) \to \Delta(\mathbf{k})/\lambda_0$, and $b(\mathbf{k}) \to b(\mathbf{k})/\lambda_0$.

To obtain the probability $p_{\mathbf{k}}$ of ending in the excited state at $t = \infty$, we study the time evolution of the system governed by the Schrödinger equation $i\partial\psi_{\mathbf{k}}/\partial t = h_{\mathbf{k}}\psi_{\mathbf{k}}$. This leads to the equations

$$\begin{aligned} i\dot{c}_{1\mathbf{k}} &= (|t/\tau|^{\alpha}\mathrm{sign}(t) + b(\mathbf{k}))\; c_{1\mathbf{k}} \;+\; \Delta(\mathbf{k})\; c_{2\mathbf{k}}, \\ i\dot{c}_{2\mathbf{k}} &= -(|t/\tau|^{\alpha}\mathrm{sign}(t) + b(\mathbf{k}))\; c_{2\mathbf{k}} \;+\; \Delta^{*}(\mathbf{k})\; c_{1\mathbf{k}}, \end{aligned} \tag{1.47}$$

where $\dot{c}_{1\mathbf{k}(2\mathbf{k})} \equiv \partial_t c_{1\mathbf{k}(2\mathbf{k})}$. To solve these equations, we define

$$\begin{aligned} c'_{1\mathbf{k}} &= c_{1\mathbf{k}}\; e^{i\int^t dt'(|t'/\tau|^{\alpha}\mathrm{sign}(t') + b(\mathbf{k}))}, \\ c'_{2\mathbf{k}} &= c_{2\mathbf{k}}\; e^{-i\int^t dt'(|t'/\tau|^{\alpha}\mathrm{sign}(t') + b(\mathbf{k}))}. \end{aligned} \tag{1.48}$$

Substituting (1.48) in (1.47) and eliminating $c'_{2\mathbf{k}}$ from the resulting equations, we get

$$\ddot{c}'_{1\mathbf{k}} \;-\; 2i\;[|t/\tau|^{\alpha}\mathrm{sign}(t) + b(\mathbf{k})]\;\dot{c}'_{1\mathbf{k}} \;+\; |\Delta(\mathbf{k})|^2\; c'_{1\mathbf{k}} \;=\; 0. \tag{1.49}$$

Now we scale $t \to t\,\tau^{\alpha/(\alpha+1)}$ so that (1.49) becomes

$$\ddot{c}'_{1\mathbf{k}} \;-\; 2i\;[|t|^{\alpha}\mathrm{sign}(t) + b(\mathbf{k})\tau^{\alpha/(\alpha+1)}]\;\dot{c}'_{1\mathbf{k}} \;+\; |\Delta(\mathbf{k})|^2\tau^{2\alpha/(\alpha+1)}\; c'_{1\mathbf{k}} \;=\; 0. \tag{1.50}$$

From (1.50) we note that since $c_{1\mathbf{k}}$ and $c'_{1\mathbf{k}}$ differ only by a phase factor, $p_{\mathbf{k}}$ must be of the form

$$p_{\mathbf{k}} \;=\; f[b(\mathbf{k})\tau^{\frac{\alpha}{\alpha+1}}, |\Delta(\mathbf{k})|^2\tau^{\frac{2\alpha}{\alpha+1}}], \tag{1.51}$$

where f is a function whose analytical form is not known for $\alpha \neq 1$. Nevertheless, we note that for a slow quench (large τ), $p_{\mathbf{k}}$ becomes appreciable only when the instantaneous energy gap, as obtained from (1.46), becomes small at some point of time during the quench. Consequently, f must vanish when either of its arguments are large: $f(\infty, a) = f(a, \infty) = 0$ for any value of a. Thus for a slow quench (large τ), the defect density n is given by

$$n \;\sim\; \int_{\rm BZ} d^dk\; f[b(\mathbf{k})\tau^{\frac{\alpha}{\alpha+1}}, |\Delta(\mathbf{k})|^2\tau^{\frac{2\alpha}{\alpha+1}}], \tag{1.52}$$

and receives its main contribution from values of f near $\mathbf{k} = \mathbf{k}_0$ where both $b(\mathbf{k})$ and $\Delta(\mathbf{k})$ vanish. Thus one obtains, after extending the range of the integration to ∞,

$$n \;\sim\; \int d^dk\; f\left[|\mathbf{k}-\mathbf{k}_0|^{z_1}\tau^{\frac{\alpha}{\alpha+1}}; |\mathbf{k}-\mathbf{k}_0|^2\tau^{\frac{2\alpha}{\alpha+1}}\right]. \tag{1.53}$$

Now scaling $\mathbf{k} \to (\mathbf{k}-\mathbf{k}_0)\tau^{\alpha/(\alpha+1)}$, we find that

$$\begin{aligned} n &\sim \tau^{-\frac{d\alpha}{\alpha+1}} \int d^dk\; f(|\mathbf{k}|^{z_1}\tau^{\alpha(1-z_1)/(\alpha+1)}; |\mathbf{k}|^2) \\ &\sim \tau^{-\frac{d\alpha}{\alpha+1}} \int d^dk\; f(0; |\mathbf{k}|^2) \;\sim\; \tau^{-\frac{d\alpha}{\alpha+1}}, \end{aligned} \tag{1.54}$$

where, in arriving at the last line, we have used $z_1 > 1$ and $\tau \to \infty$. (If $z_1 = 1$, the integral in the first line is independent of τ, so the scaling argument still holds). Note that for $\alpha = 1$, Eq. (1.54) reduces to its counterpart for a linear quench [12]. It turns out that the case $z_1 < 1$ deserves a detailed discussion which is given in Ref. [14].

Next we generalize our results to a critical point with arbitrary values of z and ν. We use arguments similar to those given in the discussion around Eq. (1.31), namely,

$$n \;\sim\; \int d^dk \left| \int_{-\infty}^{\infty} d\lambda\; \langle \mathbf{k}| \frac{d}{d\lambda} |0\rangle\; e^{i\tau \int^{\lambda} d\lambda' \delta\omega_{\mathbf{k}}(\lambda')} \right|^2. \tag{1.55}$$

In the present case, the quench term vanishes at the critical point as $\Delta \sim |\lambda|^{\alpha z\nu}$ for a nonlinear quench, and we can write

$$\delta\omega_{\mathbf{k}}(\lambda) \;=\; |\lambda|^{\alpha z\nu} \tilde{F}(|\lambda|^{\alpha z\nu}/|\mathbf{k}-\mathbf{k}_0|^z), \tag{1.56}$$

where $\tilde{F}(x) \sim 1/x$ for large x. Further, $\langle \mathbf{k}| \frac{d}{d\Delta} |0\rangle = |\mathbf{k}-\mathbf{k}_0|^{-z} G(\Delta/|\mathbf{k}-\mathbf{k}_0|^z)$ near a critical point, where $G(0)$ is a constant. This allows us to write

$$\langle \mathbf{k}| \frac{d}{d\lambda} |0\rangle \;=\; \frac{\lambda^{\alpha z\nu - 1}}{|\mathbf{k}-\mathbf{k}_0|^z} G'(\lambda^{\alpha z\nu}/|\mathbf{k}-\mathbf{k}_0|^z), \tag{1.57}$$

where $G'(0)$ is a constant [1, 12]. Substituting (1.56) and (1.57) in (1.55) and changing the integration variables to $\eta = \tau^{\alpha\nu/(\alpha z\nu+1)}|\mathbf{k}-\mathbf{k}_0|$ and $\xi = |\mathbf{k}-\mathbf{k}_0|^{-1/(\alpha\nu)}\lambda$, we find that

$$n \sim \tau^{-\alpha d\nu/(\alpha z\nu+1)}. \tag{1.58}$$

Next we consider the case where the quench term does not vanish at the QCP for $\mathbf{k} = \mathbf{k}_0$. We again consider the Hamiltonian $h_{\mathbf{k}}(t)$ in (1.45), but now assume that the critical point is reached at $t = t_0 \neq 0$. This renders our previous scaling argument invalid since $\Delta(\mathbf{k}_0) = 0$ but $b(\mathbf{k}_0) \neq 0$. In this situation, $|t_0/\tau| = g^{1/\alpha}$ so that the energy gap ΔE may vanish at the critical point for $\mathbf{k} = \mathbf{k}_0$. We now note that the most important contribution to the defect production comes from times near t_0 and from wave numbers near k_0. Hence we expand the diagonal terms in $h_{\mathbf{k}}(t)$ about $t = t_0$ and $\mathbf{k} = \mathbf{k}_0$ to obtain

$$H = \sum_{\mathbf{k}} \Big[\Big\{ \alpha g^{(\alpha-1)/\alpha} \left(\frac{t-t_0}{\tau} \right) + b'(\delta\mathbf{k}) \Big\} \sigma^3_{\mathbf{k}} + \Delta(\mathbf{k})\sigma^+_{\mathbf{k}} + \Delta^*(\mathbf{k})\sigma^-_{\mathbf{k}} \Big], \tag{1.59}$$

where $b'(\delta\mathbf{k})$ represents all the terms in the expansion of $b(\mathbf{k})$ about $\mathbf{k} = \mathbf{k}_0$, and we have neglected all terms

$$R_n = (\alpha - n + 1)(\alpha - n + 2)...(\alpha)\, g^{(\alpha-n)/\alpha} |(t-t_0)/\tau|^n \mathrm{sign}(t)/n! \tag{1.60}$$

for $n > 1$ in the expansion of $\lambda(t)$ about t_0. We shall justify neglecting these higher order terms shortly.

Eq. (1.59) describes a linear quench of the system with $\tau_{\mathrm{eff}}(\alpha) = \tau/(\alpha g^{(\alpha-1)/\alpha})$. Hence one can use the well-known results of Landau-Zener dynamics [41] to write an expression for the defect density,

$$n \sim \int_{\mathrm{BZ}} d^d k\, p_{\mathbf{k}} \sim \int_{\mathrm{BZ}} d^d k\, \exp[-\pi |\Delta(\mathbf{k})|^2 \tau_{\mathrm{eff}}(\alpha)]. \tag{1.61}$$

For a slow quench, the contribution to n comes from $\mathbf{k}$ near $\mathbf{k}_0$; hence

$$n \sim \tau_{\mathrm{eff}}(\alpha)^{-d/2} = \left(\alpha g^{(\alpha-1)/\alpha}/\tau \right)^{d/2}. \tag{1.62}$$

Note that for the special case $\alpha = 1$, we recover the familiar result $n \sim \tau^{-d/2}$, and the dependence of n on the non-universal constant g vanishes. Also, since the quench is effectively linear, we can use the results of Ref. [12] to find the scaling of the defect density when the critical point at $t = t_0$ is characterized by arbitrary z and ν,

$$n \sim \left(\alpha g^{(\alpha-1)/\alpha}/\tau \right)^{\nu d/(z\nu+1)}. \tag{1.63}$$

Next we justify neglecting the higher order terms R_n. We note that significant contributions to n come at times t when the instantaneous energy levels of H in (1.59) for a given $\mathbf{k}$ are close to each other, i.e., $(t-t_0)/\tau \sim \Delta(\mathbf{k})$. Also, for a slow quench, the contribution to the defect density is substantial only when $p_{\mathbf{k}}$ is significant, namely, when $|\Delta(\mathbf{k})|^2 \sim 1/\tau_{\mathrm{eff}}(\alpha)$. Using these arguments, we see that

$$R_n/R_{n-1} = (\alpha - n + 1) g^{-1/\alpha} (t-t_0)/(n\tau) \sim (\alpha - n + 1)/(n\sqrt{\tau}). \tag{1.64}$$

Thus we find that all higher order terms $R_{n>1}$, which were neglected in arriving at (1.62), are unimportant in the limit of slow quench (large τ).

The scaling relations for the defect density n given by (1.58) and (1.63) represent the central results of this section. For such power law quenches, unlike their linear counterpart, n depends crucially on whether or not the quench term vanishes at the critical point. For quenches which do not vanish at the critical point, n scales with the same exponent as that of a linear quench, but is characterized by a modified non-universal effective rate $\tau_{\rm eff}(\alpha)$. If, however, the quench term vanishes at the critical point, we find that n scales with a novel α-dependent exponent $\alpha d\nu/(\alpha z\nu+1)$. For $\alpha=1$, $\tau_{\rm eff}(\alpha)=\tau$ and $\alpha d\nu/(\alpha z\nu+1)=d\nu/(z\nu+1)$; hence both (1.58) and (1.63) reproduce the well-known defect production law for linear quenches as a special case [12]. We note that the scaling of n will show a cross-over between the expressions given in (1.58) and (1.63) near some value of $\tau=\tau_0$ which can be found by equating these two expressions; this yields $\tau_0 \sim |b(\mathbf{k}_0)|^{-z\nu-1/\alpha}$. For $\alpha>1$, the scaling law will thus be given by Eq. (1.58) ((1.63)) for $\tau \ll (\gg)\tau_0$. We also note here that the results of this section assumes that the system passes from one gapped phase to another through a critical point and do not apply to quenches which take a system along a critical line [13, 43, 44, 45].

To illustrate the form of defect scaling for a non-linear quench, let us consider the 1D spin-1/2 Kitaev model which is governed by the Hamiltonian

$$H \;=\; \sum_{i\in \text{even}} \left(J_1 S_i^x S_{i+1}^x \;+\; J_2 S_i^y S_{i-1}^y\right), \tag{1.65}$$

where $S_i^a=\sigma_i^a/2$. Using the standard Jordan-Wigner transformation, this can be mapped to a Hamiltonian of non-interacting fermions

$$\begin{aligned} H &= \sum_{\mathbf{k}} \psi_k^\dagger\, h_k\, \psi_k, \\ \text{where}\quad h_k &= -2\,(J_-\sin k\;\tau_3 + J_+\cos k\;\tau_2). \end{aligned} \tag{1.66}$$

Here $J_\pm = J_1 \pm J_2$, and $\psi_k=(c_1(k),c_2(k))$ are the fermionic fields. We now perform a quench by keeping J_+ fixed and varying the parameter J_- with time as $J_-(t)=J|t/\tau|^\alpha \text{sign}(t)$. We then pass through a QCP at $t=0$ at the wave number $k=\pi/2$. From Eq. (1.58) we expect the defect density to go as $n\sim\tau^{-\alpha/(\alpha+1)}$ since $\nu=z=1$ for this system. To check this prediction, we numerically solve the Schrödinger equation $i\partial\psi(k,t)/\partial t = h_k(t)\psi(k,t)$ and compute the defect density $n = \int_0^\pi (dk/\pi)\; p_k$ as a function of the quench rate τ for different α, with fixed $J_+/J=1$. A plot of $\ln(n)$ vs $\ln(\tau)$ for different values of α is shown in Fig. 1.13. The slopes of these lines, as can be seen from Fig. 1.13, changes from -0.67 towards -1 as α increases from 2 towards larger values. This behavior is consistent with the prediction of (1.58). The slopes of these lines show excellent agreement with (1.58) as shown in the inset of Fig. 1.13.

To illustrate what happens if the QCP is crossed at a time t which is different from 0, we consider the 1D Ising model in a transverse magnetic field described by

$$H_{\rm Ising} \;=\; -\;J\,(\sum_i S_i^z S_{i+1}^z \;+\; g\;\sum_i S_i^x), \tag{1.67}$$

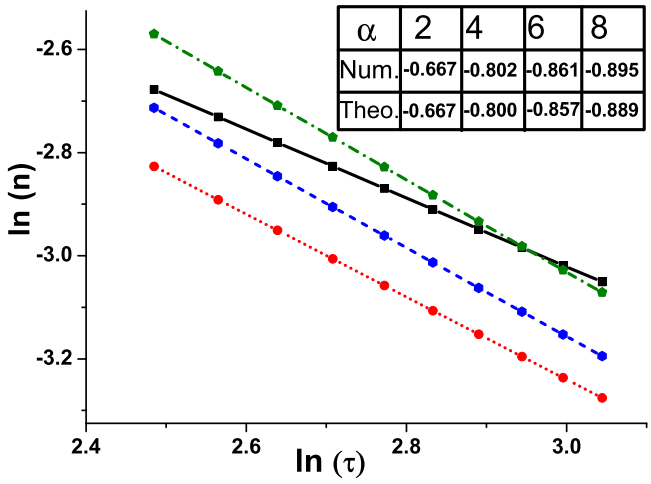

Fig. 1.13. (Color online) Plot of $\ln(n)$ vs $\ln(\tau)$ for the 1D Kitaev model for $\alpha = 2$ (black solid line), $\alpha = 4$ (red dotted line), $\alpha = 6$ (blue dashed line) and $\alpha = 8$ (green dash-dotted line). The slopes of these lines agree reasonably with the predicted theoretical values $-\alpha/(\alpha+1)$ as shown in the table.

where J is the strength of the nearest neighbor interaction, and $g = h/J$ is the dimensionless transverse field. In what follows, we shall quench the transverse field as $g(t) = |t/\tau|^{\alpha}\text{sign}(t)$ and compute the density of the resultant defects.

We begin by mapping H_{Ising} to a system of free fermions via the Jordan-Wigner transformation

$$H = -J\sum_k [(g - \cos k)\,\sigma_k^3 + \sin k\,\sigma_k^1]. \tag{1.68}$$

If the field g is varied with time as $g(t) = g_0|t/\tau|^{\alpha}\text{sign}(t)$, the system will go through two QCPs at $g = 1$ and -1. The energy gap vanishes at these QCPs at $k = k_0 = 0$ and π. As a result, defects are produced in non-adiabatic regions near these points. For this model, the QCP is at $t = t_0 \neq 0$ and $z = \nu = 1$. Hence, $\tau_{\text{eff}} = \tau/\alpha$ for both the QCPs. From (1.63), therefore, we expect the defect density produced in this system to be given by $n \sim (\tau/\alpha)^{-1/2}$.

To verify this, we numerically solve the Schrödinger equation $i\partial\psi_k(t)/\partial t = h_k(t)\psi_k(t)$ and obtain the probability p_k for the system to be in the excited state. Finally, integrating over all k within the Brillouin zone, we obtain the defect density n for different values of $\alpha > 1$ with fixed τ. The plot of n as a function of α for $\tau = 10,\ 15$ and 20 is shown in Fig. 1.14. A fit to these curves gives the values of the exponents to be 0.506 ± 0.006, 0.504 ± 0.004 and 0.505 ± 0.002 for $\tau = 10,\ 15$ and 20 respectively which are remarkably close to the theoretical value $1/2$. The systematic positive deviation of the exponents from the theoretical value $1/2$ comes from the contribution of the higher order terms neglected in the derivation of (1.62) and

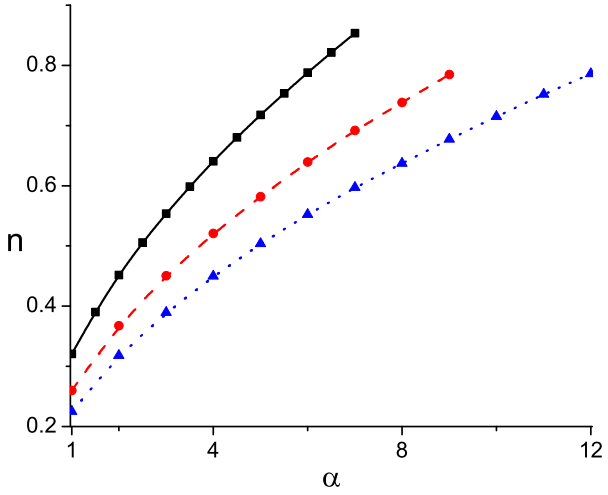

Fig. 1.14. (Color online) Variation of the defect density n with the quench exponent α for representative values of $\tau = 10$ (black solid line), $\tau = 15$ (red dashed line) and $\tau = 20$ (blue dotted line). A polynomial fit of the form $n = a\alpha^b$ yields exponents which are very close to the theoretical result $1/2$ for all values of τ.

(1.63). We note that the region of validity of our linear expansion, as can be seen from Fig. 1.14, grows with τ which is in accordance with the result in (1.64).

1.3.3 Experimental realizations

The validity of our results can be checked in a variety of experimental systems. We first observe that all our results have been obtained at zero temperature with the assumption that the system does not relax significantly during the quenching process and until the defect density has been measured. This might seem rather restrictive. We note however that systems of ultracold atoms in optical or magnetic traps and/or optical lattices can easily satisfy the required criteria since they have a very long relaxation time which often gets close to the system lifetime [38]. We will briefly list some possible experiments here. First, there has been a proposal for realizing the Kitaev model using an optical lattice[39]. In such a realization, all the couplings can be independently tuned using separate microwave radiations. In the proposed experiment, one needs to keep $J_3 = 0$ and vary $J_{1(2)} = J(1 \pm |t/\tau|^{\alpha}\text{sign}(t))/2$, so that J_+ remains constant while J_- varies in time. The variation of the defect density, which in the experimental set-up would correspond to the bosons being in the wrong spin state, would then show the theoretically predicted power law behavior in (1.58). Secondly, a similar quench experiment can be carried out with spin-1 bosons in a magnetic field described by an effective Hamiltonian $H_{\text{eff}} = c_2 n_0 \langle \mathbf{S} \rangle^2 + c_1 B^2 \langle S_z^2 \rangle$ [40], where $c_2 < 0$ and n_0 is the boson density. Such a system undergoes a quantum phase transition from a ferromagnetic state to a polar condensate at $B^* = \sqrt{|c_2| n_0 / c_1}$.

A quench of the magnetic field $B^2 = B_0^2|t/\tau|^\alpha$ would thus lead to a scaling of the defect density with an effective rate $\tau_{\rm eff}(\alpha) = \tau/(\alpha g^{(\alpha-1)/\alpha})$, where $g = |c_2|n_0/c_1$. A measurement of the dependence of the defect density n on α should therefore serve as a test of the prediction in (1.63). Finally, spin gap dimer compounds such as $BaCuSi_2O_6$ are known to undergo a singlet-triplet quantum phase transition of the Bose-Einstein condensation type at $B_c \simeq 23$T; the critical exponents for this are given by $z = 2$ and $\nu = 2/d$. Experimentally, the exponent ν appears to be $2/3$ above a temperature window of 0.65K to 0.9K [54] and 1 below that temperature window due to a dimensional reduction from $d = 3$ to $d = 2$ [55]. Thus a nonlinear quench of the magnetic field through its critical value $B = B_c + B_0|t/\tau|^\alpha {\rm sign}(t)$ should lead to a scaling of the defects $n \sim \tau^{-6\alpha/(4\alpha+3)}$ for $d = 3$, $\nu = 2/3$, and $n \sim \tau^{-2\alpha/(2\alpha+1)}$ for $d = 2$, $\nu = 1$. It would be interesting to see if the defect scaling exponent depends on the temperature range in the same way as the exponent ν. In the experiment, the defect density would correspond to residual singlets in the final state which can be computed by measuring the total magnetization of the system immediately after the quench. We note that for these dimer systems, it would be necessary to take special care to achieve the criterion of long relaxation time mentioned earlier.

1.4 Quantum communication

In this section, we demonstrate that a properly engineered non-adiabatic dynamics may lead to larger fidelity and higher speed for the transfer of a qubit through a system. For this purpose, we begin with a Heisenberg spin-1/2 chain described by a generic time-dependent Hamiltonian

$$H \;=\; -J_0(t)\,\sum_{ij}(S_i^x S_j^x + S_i^y S_j^y) \;+\; \Delta(t)\sum_{ij} S_i^z S_j^z \;+\; B(t)\,\sum_i S_i^z. \tag{1.69}$$

We assume that the spin system is on a ring with N sites. We start with the initial ground state being ferromagnetic, and denote this state by $|G\rangle$. At the start of the procedure of qubit transfer, we put a state $\cos(\theta/2)|\uparrow\rangle + \sin(\theta/2)\exp(i\phi)|\downarrow\rangle$ at the $r^{\rm th}$ site of the chain. Thus the initial state of the system at the start of the evolution is [15]

$$|\psi_{\rm in}\rangle \;=\; \cos(\theta/2)|G\rangle + \sin(\theta/2)e^{i\phi}|r\rangle, \tag{1.70}$$

where $|r\rangle$ denotes the state of the spin chain with one flipped spin at the site r. We now consider the evolution of this state under a time-dependent Hamiltonian H. The specific form of the interaction need not be specified at the moment. Since the total spin is a conserved quantity ($[\sum_i S_i^z, H] = 0$), the state of the system at time t becomes

$$\begin{aligned} |\psi(t)\rangle \;&=\; \cos(\theta/2)|G\rangle + \sin(\theta/2)e^{i\phi}\sum_n f_{nr}(t)|n\rangle, \\ \text{where}\quad f_{nr}(t) \;&=\; \langle n|e^{-i\int^t H(t')dt'}|r\rangle. \end{aligned} \tag{1.71}$$

Since the idea of communication through the chain involves performing measurement on the state at site s^{th} site, we would like to compute the reduced density matrix of this site at time t. To this end, we write the wave function

$$|\psi(t)\rangle = \cos(\theta/2)|G\rangle + \sin(\theta/2)e^{i\phi}\sum_{n\neq s} f_{nr}(t)|n\rangle + \sin(\theta/2)e^{i\phi} f_{sr}(t)|s\rangle, \quad (1.72)$$

where the first line of the last equation is the contribution from all terms to $|\psi(t)\rangle$ where the spin in the s^{th} site is $\uparrow$. Note that for normalization of the wave function, one needs

$$\cos^2(\theta/2) + \sin^2(\theta/2)\sum_{n\neq s}|f_{nr}(t)|^2 = 1 - |f_{sr}(t)|^2\sin^2(\theta/2). \quad (1.73)$$

Using (1.72) and (1.73), one find that the reduced density matrix for the s^{th} site of the system is

$$\begin{aligned}\rho_s(t) = {} & (1-|f_{sr}(t)|^2\sin^2(\theta/2))\,|\uparrow\rangle\langle\uparrow| + |f_{sr}(t)|^2\sin^2(\theta/2)\,|\downarrow\rangle\langle\downarrow| \\ & + \frac{\sin(\theta)}{2}\left(e^{i\phi}f_{sr}(t)|\downarrow\rangle\langle\uparrow| + e^{-i\phi}f_{sr}^*(t)|\uparrow\rangle\langle\downarrow|\right). \end{aligned} \quad (1.74)$$

The fidelity of the state transfer at the given time t is thus defined as [15]

$$\begin{aligned} F(t) &= \frac{1}{4\pi}\int d\Omega\,\langle\psi_{\text{in}}|\rho_s(t)|\psi_{\text{in}}\rangle \\ &= \frac{1}{2} + \frac{|f_{sr}(t)|^2}{6} + \frac{Re[f_{rs}(t)]}{3}, \end{aligned} \quad (1.75)$$

where the integration is over the Bloch sphere involving θ and ϕ. Thus to obtain the fidelity of a state transfer we need to obtain the matrix elements $f_{sr}(t)$. To do this, we note that since the Hamiltonian in (1.69) conserves the z component of the spin, an arbitrary time-dependent dynamics always restricts the system to lie within the subspace of one flipped spin. This allows us to write the wave function after an evolution through a time t to be

$$|\phi(t)\rangle = \sum_n c_n(t)|n\rangle = \sum_k c_k(t)|k\rangle, \quad (1.76)$$

where the real space basis $|n\rangle$ and the wave number space basis $|k\rangle$ are related by $|n\rangle = \sum_k \exp(-ikn)|k\rangle$ for a chain with a periodic boundary condition. The Schrödinger equation for $|\phi(t)\rangle$ now leads to the following equation for $c_k(t)$

$$i\dot{c}_k(t) = \left(2J(t)\cos(k) + \frac{1}{4}[\Delta(t) + 2B(t)]\right)c_k(t), \quad (1.77)$$

where we have neglected factors of $1/N$ (N being the chain length which approaches infinity in the thermodynamic limit) in the expression for $\beta(t)$. These equations are to be solved with the boundary condition $c_n(t=0) = \delta_{nr}$. This equation has a straightforward solution

$$c_k(t) = e^{-i(2\alpha(t)\cos(k)+\beta(t))},$$
$$\text{where} \quad \alpha(t) = \int^t J(t')dt', \quad \text{and} \quad \beta(t) = \int^t \frac{1}{4}[\Delta(t') + 2B(t')]dt'. \quad (1.78)$$

Using (1.78), one gets

$$f_{sr}(t) = \langle s|e^{-i\int^t H(t')dt'}|r\rangle = \langle s|\phi(t)\rangle$$
$$= \sum_k e^{-i[k(r-s)+2\alpha(t)\cos(k)+\beta(t)]}. \quad (1.79)$$

For an infinite chain, the momentum sum can be converted to an integral and exactly evaluated to yield

$$f_{sr}(t) = J_{r-s}(2\alpha(t))\, e^{-i\beta(t)}. \quad (1.80)$$

From this result, we note the following points. First, we need to choose a time when we shall perform a measurement on the state. This time, t_0, is chosen so as to maximize the fidelity of the state transfer. In the present model, this occurs at the time t_0 when the argument $2\alpha(t_0)$ of the Bessel function approximately equals $r-s$. This suggests that one can reach the maximum fidelity (i.e., maximum $|f_{sr}(t)|$ and maximum $Re[f_{sr}(t)]$ which requites a separate adjustment of the phase factor) for a given separation $r-s$ at a much shorter time for a suitable non-adiabatic dynamics. This ensures faster communication through the channel. Note that by choosing an appropriate form of $J(t)$, the communication can be made exponentially faster compared to adiabatic dynamics since we may ramp up the effective instantaneous velocity so that a given separation $r-s$ is reached at a much shorter time. Second, the non-adiabatic dynamics gives us an additional handle on the phase and hence the real part of $f_{sr}(t)$. Thus one can adjust the phase using a user-chosen classical control parameter (such as frequency in the case of AC dynamics) to obtain maximum fidelity for a given $|f_{sr}(t)|$. Finally, it is straightforward to generalize the derivation of $f_{sr}(t)$ to higher dimensions. The result for a 2D system is

$$f_{\mathbf{sr}} = J_{r_x-s_x}(2\alpha(t))\, J_{r_y-s_y}(2\mu\alpha(t))\, e^{-i\beta(t)}, \quad (1.81)$$

where μ is an anisotropy parameter which signifies the relative strengths of couplings of the S_x and S_y terms in the two orthogonal spatial directions. For $\mu = 1$, i.e., the isotropic case, we find that the fidelity is maximized when propagation takes place along the diagonal. But in general, the angle of maximum propagation is a function of μ and this can in general also be controlled. A similar analysis can be easily extended to higher dimensions; however, as can be seen from (1.81), the fidelity of the qubit transfer using this method rapidly decays with increasing dimensions.

Thus we find, via a simple analysis of a Heisenberg spin model with a time-dependent Hamiltonian, that both the fidelity and the speed of quantum communication may be improved by using suitable non-equilibrium dynamics. We have also shown that such a procedure can lead to direction specific state transfer in higher dimensional spin systems. Since engineering such time-dependent Hamiltonians have become an experimental reality, this might, in principle, provide a realizable way for faster communication of qubits in future experiments.

1.5 Discussion

To summarize, we first discussed the response of a system of interacting bosons in a 1D optical lattice to a sudden change in a harmonic trap potential. The system can be mapped to a system of dipoles described by an Ising order parameter. After the sudden shift, the order parameter oscillates in time; the amplitude of oscillations depends on the initial and final trap potentials. We then considered an infinite range ferromagnetic Ising model in a transverse magnetic field; we studied what happens after the field is changed suddenly. Once again, the variation of the order parameter (the magnetization in this problem) with time depends in an interesting way on the initial and final fields and the system size.

Next, we considered what happens when a system is taken across a quantum critical point or a critical surface in a non-adiabatic way which is governed by a quench time τ. This leads to the production of defects; the density of defects scales as an inverse power of τ, where the power depends on the dimensionalities of the system and the critical surface and the critical exponents z and ν. This was illustrated by considering the Kitaev model which is an exactly solvable spin-1/2 model defined on the honeycomb lattice; this can be solved by mapping it to a system of non-interacting Majorana fermions using a Jordan-Wigner transformation. We then considered the effect of taking a system across a QCP in a non-linear manner at time $t = 0$; the non-linearity is parametrized by an exponent α. We found that two different things happen depending on whether the system passes through the QCP at $t = 0$ or at a non-zero value of t. In the former case, the power appearing in the scaling of the defect density with τ also depends on α; in the latter case, the power is the same as in a linear quench (corresponding to $\alpha = 1$), but the effective quench time $\tau_{\rm eff}$ depends on α. These ideas are illustrated by considering two models in 1D, namely, a 1D version of the Kitaev model, and the Ising model in a transverse magnetic field; both of these can solved by mapping them to systems of non-interacting fermions by a Jordan-Wigner transformation. We then discussed some experimental systems where our results for the defect scaling can be checked.

Finally, we used some Heisenberg spin-1/2 models in one and two dimensions to discuss how a qubit can be transferred across the system. In particular, we examined how the speed and fidelity of the transfer can be maximized by choosing the couplings in the Hamiltonian appropriately.

Before ending, we would like to mention two possible extensions of the work discussed here. First, it would be interesting to study whether the defects studied in Sect. 1.3 have any non-trivial topology associated with them. If they are not topological, it would be interesting to find other ways of changing the parameters in the Hamiltonian in order to produce defects which do have a topological character. It is known that topology can affect defect production in a profound way [56]. Secondly, the defect density discussed in Sect. 1.3 follows from the density matrix of a single site obtained by integrating out all the other sites of the system. It is interesting to compute the two-site density matrix and use that to obtain various measures of two-site entanglement. This has been studied recently both for a sudden quench [57] and

a slow quench [58] through a QCP. Other kinds of entanglement produced due by a quench have also been studied [59].

Acknowledgements

We thank Amit Dutta and Anatoli Polkovnikov for stimulating discussions.

References

1. S. Sachdev, *Quantum Phase Transitions* (Cambridge University Press, Cambridge, 1999).
2. S. K. Ma, *Modern Theory of Critical Phenomena* (Addison-Wesley, New York, 1996).
3. K. Damle and S. Sachdev, Phys. Rev. B **56**, 8714 (1997); S. Sachdev and K. Damle, Phys. Rev. Lett. **78**, 943 (1997); S. A. Hartnoll, P. K. Kovtun, M. Müller and S. Sachdev, Phys. Rev. B **76**, 144502 (2007); A. Del Maestro, B. Rosenow, N. Shah and S. Sachdev, Phys. Rev. B **77**, 180501(R) (2008).
4. K. Sengupta, S. Powell and S. Sachdev, Phys. Rev. A **69**, 053616 (2004).
5. R. A. Barankov and L. S. Levitov, Phys. Rev. Lett. **96**, 230403 (2006).
6. A. A. Burkov, M. D. Lukin and E. Demler, Phys. Rev. Lett. **98**, 200404 (2007); R. W. Cherng, V. Gritsev, D. M. Stamper-Kurn and E. Demler, Phys. Rev. Lett. **100**, 180404 (2008).
7. E. Altman, A. Polkovnikov, E. Demler, B. Halperin and M. D. Lukin, Phys. Rev. Lett. **95**, 020402 (2005); V. Gritsev, E. Demler, M. Lukin and A. Polkovnikov, Phys. Rev. Lett. **99**, 200404 (2007).
8. A. Das, K. Sengupta, D. Sen and B. K. Chakrabarti, Phys. Rev. B **74**, 144423 (2006).
9. M. Greiner, O. Mandel, T. Esslinger, T. W. Hänsch and I. Bloch, Nature **415**, 39 (2002); for a review, see I. Bloch, Nature Physics **1**, 23 (2005).
10. T. W. B. Kibble, J. Phys. A **9**, 1387 (1976); W. H. Zurek, Nature **317**, 505 (1985).
11. N. D. Antunes, L. M. A. Bettencourt and W. H. Zurek, Phys. Rev. Lett. **82**, 2824 (1999); J. Dziarmaga, P. Laguna and W. H. Zurek, Phys. Rev. Lett. **82**, 4749 (1999); J. R. Anglin and W. H. Zurek, Phys. Rev. Lett. **83**, 1707 (1999).
12. A. Polkovnikov, Phys. Rev. B **72**, 161201(R) (2005).
13. K. Sengupta, D. Sen and S. Mondal, Phys. Rev. Lett. **100**, (2008) 077204; S. Mondal, D. Sen and K. Sengupta, Phys. Rev. B **78**, (2008) 045101.
14. D. Sen, K. Sengupta and S. Mondal, Phys. Rev. Lett. **101**, (2008) 016806; S. Mondal, K. Sengupta and D. Sen, Phys. Rev. B **79**, (2009) 045128.
15. S. Bose, Phys. Rev. Lett. **91**, 207901 (2003).
16. M. Christandl, N. Datta, A. Ekert and A. J. Landahl, Phys. Rev. Lett. **92**, 187902 (2004); C. Albanese, M. Christandl, N. Datta and A. Ekert, Phys. Rev. Lett. **93**, 230502 (2004); M. Christandl, N. Datta, T. Dorlas, A. Ekert, A. Kay and A. Landahl, Phys. Rev. A **71**, 032312 (2005); A. Kay, Phys. Rev. Lett. **98**, 010501 (2007).
17. S. Sachdev, K. Sengupta and S. M. Girvin, Phys. Rev. B **66**, 075128 (2002).
18. S. Dusuel and J. Vidal, Phys. Rev. Lett. **93**, 237204 (2004); *ibid*, Phys. Rev. B **71**, 224420 (2005); J. Vidal, G. Palacios and J. Aslangul, Phys. Rev. A **70**, 062304 (2004).
19. B. K. Chakrabarti and J.-I. Inoue, Ind. J. Phys. **80**, 609 (2006); B. K. Chakrabarti, A. Das and J.-I. Inoue, Euro. Phys. J. B **51**, 321 (2006).
20. E. Fradkin, *Field Theories of Condensed Matter Systems* (Addison-Wesley, Reading, 1991).

21. B. K. Chakrabarti, A. Dutta and P. Sen, *Quantum Ising Phases and Transitions in Transverse Ising Models* (Springer, Heidelberg, 1996).
22. D. Gordon and C. M. Savage, Phys. Rev. A **59**, 4623 (1999).
23. A. Micheli, D. Jaksch, J. I. Cirac and P. Zoller, Phys. Rev. A **67**, 013607 (2003); A. P. Hines, R. H. McKenzie and G. J. Milburn, Phys. Rev. A **67**, 013609 (2004).
24. A. Simoni, F. Ferlaino, G. Roati, G. Modugno and M. Inguscio, Phys. Rev. Lett **90**, 163202 (2003).
25. J. Cirac, M. Lewenstein, K. Molmer and P. Zoller, Phys. Rev. A **57**, 1208 (1998).
26. B. Damski, Phys. Rev. Lett. **95**, 035701 (2005); W. H. Zurek, U. Dorner and P. Zoller, Phys. Rev. Lett. **95**, 105701 (2005).
27. A. Polkovnikov and V. Gritsev, Nature Physics **4**, 477 (2008).
28. J. Dziarmaga, Phys. Rev. Lett. **95**, 245701 (2005), and Phys. Rev. B **74**, 064416 (2006).
29. P. Calabrese and J. Cardy, J. Stat. Mech: Theory Expt P04010 (2005), and Phys. Rev. Lett. **96**, 136801 (2006).
30. R. W. Cherng and L. Levitov, Phys. Rev. A **73**, 043614 (2006).
31. B. Damski and W. H. Zurek, Phys. Rev. A **73** 063405 (2006).
32. T. Caneva, R. Fazio and G. E. Santoro, Phys. Rev. B **76**, 144427 (2007).
33. V. Mukherjee, U. Divakaran, A. Dutta and D. Sen, Phys. Rev. B **76**, 174303 (2007).
34. F. M. Cucchietti, B. Damski, J. Dziarmaga and W. H. Zurek, Phys. Rev. A **75**, 023603 (2007).
35. C. Kollath, A. M. Lauchli and E. Altman, Phys. Rev. Lett. **98**, 180601 (2007).
36. M. Eckstein and M. Kollar, Phys. Rev. Lett. **100**, 120404 (2008).
37. S. R. Manmana, S. Wessel, R. M. Noack and A. Muramatsu, Phys. Rev. Lett. **98**, 210405 (2007).
38. For a review, see I. Bloch, J. Dalibard and W. Zwerger, Rev. Mod. Phys. **80**, 885 (2008).
39. L.-M. Duan, E. Demler and M. D. Lukin, Phys. Rev. Lett. **91**, 090402 (2003); A. Micheli, G. K. Brennen and P. Zoller, Nature Physics **2**, 341 (2006).
40. L. E. Sadler, J. M. Higbie, S. R. Leslie, M. Vengalattore and D. M. Stamper-Kurn, Nature **443**, 312 (2006).
41. See for example, L. Landau and E. M. Lifshitz, *Quantum Mechanics: Non-relativistic Theory*, 2nd Ed. (Pergamon Press, Oxford, 1965); C. Zener, Proc. Roy. Soc. London, Ser. A **137**, 696 (1932).
42. R. Barankov and A. Polkovnikov, Phys. Rev. Lett. **101**, 076801 (2008); C. De Grandi, R. A. Barankov, and A. Polkovnikov, Phys. Rev. Lett. **101**, 230402 (2008).
43. F. Pellegrini, S. Montangero, G. E. Santoro and R. Fazio, Phys. Rev. B **77**, 140404(R) (2008).
44. U. Divakaran, A. Dutta and D. Sen, Phys. Rev. B **78**, 144301 (2008).
45. U. Divakaran, V. Mukherjee, A. Dutta and D. Sen, J. Stat. Mech. (2009) P02007.
46. A. Kitaev, Ann. Phys. **321**, 2 (2006).
47. X.-Y. Feng, G.-M. Zhang and T. Xiang, Phys. Rev. Lett. **98**, 087204 (2007).
48. G. Baskaran, S. Mandal and R. Shankar, Phys. Rev. Lett. **98**, 247201 (2007).
49. D.-H. Lee, G.-M. Zhang and T. Xiang, Phys. Rev. Lett. **99**, 196805 (2007).
50. K. P. Schmidt, S. Dusuel and J. Vidal, Phys. Rev. Lett. **100**, 057208 (2008).
51. H.-D. Chen and Z. Nussinov, J. Phys. A **41**, 075001 (2008).
52. Z. Nussinov and G. Ortiz, Phys. Rev. B **77**, 064302 (2008).
53. A. Kitaev, Ann. Phys. **303**, 2 (2003).
54. S. E. Sebastian, P. A. Sharma, M. Jaime, N. Harrison, V. Correa, L. Balicas, N. Kawashima, C. D. Batista and I. R. Fisher, Phys. Rev. B **72**, 100404(R) (2005).
55. S. E. Sebastian, N. Harrison, C. D. Batista, L. Balicas, M. Jaime, P. A. Sharma, N. Kawashima and I. R. Fisher, Nature **441**, 617 (2006).

56. A. Bermudez, D. Patanè, L. Amico and M. A. Martin-Delgado, Phys. Rev. Lett. **102**, 135702 (2009).
57. A. Sen(De), U. Sen and M. Lewenstein, Phys. Rev. A **72**, 052319 (2005); H. Wichterich and S. Bose, arXiv:0806.4568v2 (unpublished).
58. K. Sengupta and D. Sen, arXiv:0904.1059 (unpublished).
59. L. Cincio, J. Dziarmaga, M. M. Rams and W. H. Zurek, Phys. Rev. A **75**, 052321 (2007); S. Deng, L. Viola and G. Ortiz, Proc. of the 14th International Conference on Recent Progress in Many-Body Theories, Series on Advances in Many-Body Theory, Vol. 11 (World Scientific, 2008), pp. 387 - 397.